Bonding Models for Ligated and Bare Clusters

D. M. P. MINGOS,* TOM SLEE, and LIN ZHENYANG

Inorganic Chemistry Laboratory, University of Oxford, South Parks Road, Oxford, OX1 3QR, England

Received July 25, 1989 (Revised Manuscript Received October 13, 1989)

Contents

I. Introduction

Although the first example of a transition-metal cluster compound was discovered more than 50 years ago, it was not until the early 1960s, when three-circle X-ray diffractometers became generally available, that this area of chemistry began to emerge as a major subdiscipline. These clusters, which can be obtained in gram quantities by conventional synthetic chemistry techniques, have a protective sheath of ligands coordinated to the metal atoms. This ligand shell confers solubility in organic solvents on the cluster and also prevents cluster aggregation to the bulk metal. For transition-metal clusters these ligands can be either π acceptors (e.g., CO, CNR, NO) or π donors (e.g., Cl, OR, S) and for main-group clusters they are generally hydrogen or an organic alkyl group.

Examples of ligated clusters with up to 44 metal atoms have been characterized in the solid state by single-crystal X-ray crystallographic techniques.[1] This has provided detailed structural information on the geometries and bond lengths associated with both the metal cluster and the ligand shell. The structures of the compounds in solution have been investigated by infrared and NMR spectroscopic techniques, and such studies have established that in many of these compounds the ligands migrate over the surface of the cluster rapidly on the NMR time scale. There are also a few examples where the metal core is stereochemically nonrigid, in particular with the gold phosphine clusters, $[Au(AuPR_3)_n]^{x+}$. These spectroscopic techniques have also provided a basis for defining the products of reactions of these clusters with a wide variety of substrates, e.g., hydrogen, unsaturated organic and inorganic molecules, etc. In addition, a reasonable understanding of the electronic structures of these clusters has emerged as a result of the combination of molecular orbital calculations and photoelectron spectral studies.

More recently, physicists and physical chemists have shown an interest in clusters formed in molecular beam experiments.[2] The study of clusters in the gas phase can be traced to the pioneering work of Schumacher and co-workers,[3] Foster and Leckenby,[4] and Echt, Recknagel, and Sattler,[5] although several other groups, mentioned below, have also contributed substantially to the development of the field. These clusters were originally generated in the gas phase by high-temperature techniques and analyzed by mass spectrometry.[5,6] In addition, Knudsen cell methods were used to study the energetics of the vapor equilibria involving the metal clusters. The study of very small clusters (two and three atoms) with low internal temperatures by modern spectroscopic methods has yielded high-resolution data concerning their electronic structures.[7,8] The molecular beam experiments combine a means of producing metal vapors at elevated temperatures with the techniques of rarefied gas dynamics to produce an isentropic and supersonically expanded "free jet" of "cold" metal clusters which are probed by mass spectrometry and laser spectroscopy.

Alternatively, metal vaporization in an inert carrier gas stream leads to a "quenching" of the metal vapor.[9] This leads to large supersaturation ratios and rapid nucleation and cluster growth.[10] Mass spectrometry, fluorescence excitation spectroscopy using tunable dye lasers, and multiphoton ionization spectroscopy have provided particularly useful information concerning cluster stability and electronic structure.[11] Photodissociation on neutrals and photodetachment of electrons from mass-selected anions are other techniques that have been applied.[12] In early experiments it was established that sodium clusters exhibit distinct "magic numbers" indicating cluster nuclearities with high stabilities relative to neighboring clusters. In particular, large mass spectral peaks corresponding to n = 8, 20, 40, 58, and 92 have been associated with clusters of high stability.[13] This observation has been rationalized by using the spherical jellium model, a simple one-electron spherical potential model.[13] Such studies have been subsequently extended to a wide range of metals and main-group atoms. Finally, reactivity studies have recently yielded information on the size dependence of the chemical behavior of clusters.[14]

The major aim of this review is to provide a theoretical framework applicable to both gas-phase bare clusters and condensed-phase ligated clusters. In particular, we shall demonstrate that although chemists

0009-2665/90/0790-0383$09.50/0

Michael Mingos is a lecturer in Inorganic Chemistry at the University of Oxford and a Fellow of Keble College, Oxford. He graduated from the Universities of Manchester (B.Sc., 1965) and Sussex (D.Phil., 1968). His doctoral research was supervised by Prof. Joseph Chatt FRS. After postdoctoral work with Profs. James Ibers and Sir Ronald Mason, he was appointed to a lectureship at Queen Mary College, University of London (1971). He has been in Oxford since 1976.

Tom Slee received his B.Sc. from the University of Sussex in 1981 and his Ph.D. from McMaster University in 1987. His Ph.D. work was on the charge density based theory of atoms in molecules developed in the laboratory of his supervisor, R. F. W. Bader. Following a year pursuing interests outside chemistry, he carried out one year of postdoctoral work with D. M. P. Mingos, where the work discussed in the present article was done. He is now doing further postdoctoral work at the University of Waterloo with R. J. Le Roy on the theory of van der Waals complexes.

Lin Zhenyang was born in Fujian, People's Republic of China, in 1962. He received his B.Sc. degree in chemistry from the Wuhan University of Geology in 1982 and his M.Sc. degree in 1985 from the Fujian Institute of Research on the Structure of Matter, Chinese Academy of Sciences. His D.Phil work was carried out in the Inorganic Chemistry Laboratory of the University of Oxford from October 1986 to August 1989 under the supervision of Dr. D. M. P. Mingos. He is now doing postdoctoral work at Texas A&M University with Professor M. B. Hall.

and physicists have developed models that superficially appear to be very different, there are many points of similarity and the conclusions derived from them are frequently identical. The review consists of two major parts: the first, a comparison of the jellium and LCAO approaches, and the second, the application of electron-counting rules to molecular beam clusters.

II. Models for Simple Metal Clusters

A. The Spherical Jellium Model

The "magic numbers" oberved in molecular beam experiments are particularly evident in the mass spectral data for alkali-metal clusters, noble gases, and carbon clusters, although the occurrence of clusters of particular stability is, as we shall see, considerably wider than this. In this section we are concerned with the alkali metals. In this group, mass spectra have been reported for Li,[15] Na,[13] K,[16,17] LiK_x,[18] Li_xNa_y,[19] Rb_xCs_y,[20] and Na_xK.[16]

Theoretical studies of the stabilities and structures of alkali-metal clusters have been of four types. Hückel calculations have been carried out on all possible neutral and cationic structures up to M_9 and on several cluster structures up to M_{14}[21,22] as well as on anions up to M_7.[23] Several aspects of the results have been analyzed: notably the orbital energies, electronic shell structures, and ionization potentials. In addition, some extrapolations to the bulk limit have been made. Calculations based on interatomic potentials have also been reported.[24] More accurate calculations using both ab initio[25] and local spin density,[26] or Xα, methods have been carried out on small lithium and sodium clusters, including some geometries up to M_{20},[27] and the results provide more detailed information on the geometries and stabilities of the smaller lithium clusters and some sodium clusters. These calculations along with many others have been reviewed recently by Koutecky and Fantucci.[25]

The simplest model is the spherical jellium model of Knight et al.,[13] which has successfully predicted several of the magic numbers for alkali-metal clusters by associating these nuclearities with closed-shell electron counts. This model postulates that the electronic structure of free-electron metal clusters may be approximately described by considering only the energies of the valence electrons in a smooth potential, without specific information about the positions of the atomic cores.

The original investigation[13] of Knight and co-workers employed a central field potential of the form

$$V_0(r) = \frac{-U_0}{\exp\left(\frac{r - r_0}{\epsilon}\right) + 1} \qquad (1)$$

where U_0 is the sum of the Fermi energy and the work function of the bulk and r_0 is the effective radius of the cluster sphere and assumed to be $r_sN^{1/2}$, where r_s is the radius of a sphere containing one electron in the bulk. The parameter ϵ was taken as 1.5 au in their calculations. This potential is a finite well with rounded sides and is illustrated in Figure 1.

This potential is also used in nuclear physics shell models, where it goes under the name of the Woods–

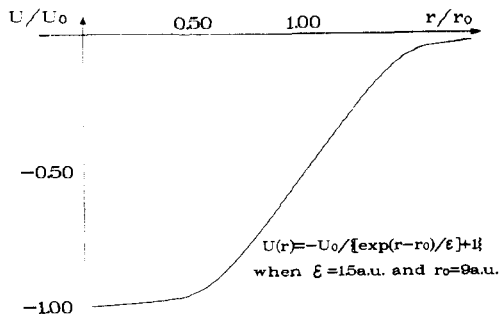

Figure 1. Woods-Saxon central field potential used by Knight et al. in their spherical jellium model of cluster electronic structure.

Saxon potential[28] and has no a priori justification in the context of clusters. Many of the jellium model conclusions are insensitive to the precise form of the central field potential, and Knight and co-workers have explored other forms of potential, including perturbed harmonic oscillator and rectangular potential well potentials.[29]

A crucial feature of the model is the separation of the Schrödinger equation into radial and angular parts, for it is this separation that yields the shell structure. The angular solutions are the spherical harmonics, which we shall meet many times during the course of this article, so the jellium wave functions can be written

$$\psi_{nlm} = f_{nl}(r) Y_l^m(\theta,\phi) \qquad (2)$$

where $Y_l^m(\theta,\phi)$ is a spherical harmonic and $f_{nl}(r)$ depends on the form of the central field potential. The wave function can thus be labeled by a principal quantum number (n) and the angular quantum numbers (l and m). In Knight's contributions, the energy level order for this one-electron model that results is[13]

$$1s < 1p < 1d < 2s < 1f < 2p < 1g < 2d < 3s < 1h...$$

(note that for non-Coulombic potentials the wave function is conventionally written so that a given n has all positive integers l associated with it). Each shell, specified by n and l, has an orbital degeneracy of $(2l + 1)$, the individual states being labeled by m. Electronic shell closings thus occur for the Woods–Saxon potential at 2, 8, 18, 20, 34, 40, 58, 68, 70, 92, ... Mass spectra revealed large peaks for masses corresponding to n = 2, 8, 20, 40, 58, and 92 atoms for neutral sodium and potassium clusters generated in gas evaporation experiments, as shown in Figure 2.[13] All these values are consistent with the spherical jellium model.

Subsequently, the spherical jellium model has been applied to rationalize the mass spectral patterns derived from charged alkali-metal clusters and from other elements. Recently reported sodium cation spectra contained large peaks at n = 19, 21, 35, and 41—also values predicted by the model.[30] Several peaks in the mass spectra of Cu, Ag, Au,[31] Zn, and Cd[32] have also been assigned to jellium closed shells.

A chemist may find the ordering of levels unfamiliar compared, for example, with the hydrogen-like atom energy levels, i.e.

$$1s < 2s < 2p < 3s < 3p < 4s < 3d < 4p...$$

The potential is, however, different in the two cases. The hydrogen-like central potential is infinite at the origin, falling off slowly (as $1/r$) with distance. In

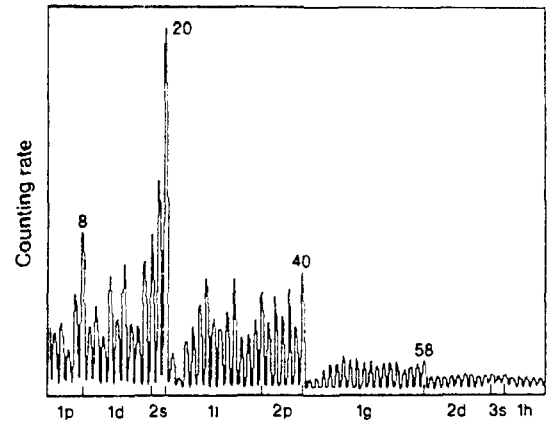

Figure 2. Mass spectrum for sodium clusters showing discontinuities at jellium "shell-closing" numbers 8, 20, 40, and 58. Adapted from: Knight, W. D.; Clemenger, K.; de Heer, W. A.; Saunders, W.; Chou, M. Y.; Cohen, M. L. *Phys. Rev. Lett.* **1984**, *52*, 2124.

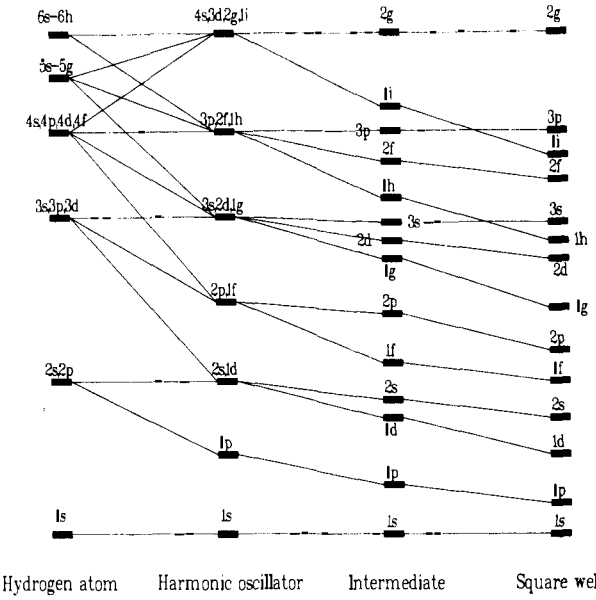

Figure 3. Energy level diagram showing energy level orderings for the hydrogen atom, the harmonic oscillator, the rounded square well, and the square well. The Woods–Saxon potential of Knight et al. and the perturbed oscillator of Clemenger both correspond to the "intermediate" case.

contrast, the jellium potential is essentially flat out to the outer spherical surface of the cluster, which is modeled as a rounded square well, as shown in Figure 1. This is very similar to a particle-in-a-sphere model. Chemists have previously used such an approach for interpreting the spectral properties of solvated electrons, where the electron is thought to be trapped in a spherical cavity. The s solutions are the only ones with nonzero density at the origin and so are greatly stabilized in the hydrogen atom as compared to the particle-in-a-sphere case. p functions are likewise stabilized compared to functions of higher angular momentum, as can be seen by comparing the ordering in the two cases. Figure 3 shows the relation between the energy level orderings for the hydrogen atom, the square well, and the isotropic harmonic oscillator, which is intermediate in character.

It has become customary to refer to a set of orbitals specified by n and l, e.g., 2p, as a *shell* in a jellium context, even though the word is used for a collection specified only by the principal quantum number n in

an atomic context. We employ the jellium terminology throughout this review.

There has been debate over the significance and usefulness of the spherical jellium model.[18] Such a simple model does, of course, have several weaknesses and limitations. In particular, although the model mades predictions concerning the electronic structure of those clusters with "closed shells" (and so could be expected to yield ionization energies, for instance, for these clusters; these predictions turn out to be inaccurate[18]), it does not make accurate predictions concerning the electronic structure of "nonmagic number" clusters. The approximation of a spherical potential leads to stable configurations for closed shells, but for nonclosed-shell clusters, for which there is no such stability, we may expect the potential to alter "shape". Such a distortion perturbs the electronic energy levels, splitting the high degeneracy associated with spherical symmetry. Such a splitting would be expected to stabilize clusters with partially filled shells.

Second, the model often predicts too many "magic numbers". The electronic closed-shell requirement appears to be a necessary, but not sufficient, condition for the spherical stability associated with "magic numbers": how can be explain which closed shells will be observed as magic numbers and which will not? A third limitation is that the energy level ordering of the Woods–Saxon potential, which fits the alkali-metal spectra so well, does not fit the observations for several mixed, or compound, clusters. For instance, the Mg_xK_y system has been studied[18] and shows evidence for a particularly stable cluster at ten valence electrons: MgK_8. This suggests that the 2s shell is brought down in energy below the 1d shell in this system.[33,34] Finally, if we are interested in a more detailed analysis of the properties of alkali-metal clusters, we need to have more information concerning their structures. The spherical jellium model provides little guide for us in this, even for closed-shell clusters.

These limitations have prompted extensions to the original spherical jellium model. Electron–electron interaction has been included in the spherical jellium model by Ekardt.[35,36] Baladron and Alonso[37] replaced the Woods–Saxon potential with a background positive charge density of spherical symmetry but varying with radial distance from the center in order ot explain the electronic structure of closed-shell compound clusters such as MgK_8. Clemenger[38] removed the restriction of spherical symmetry, employing a perturbed harmonic oscillator model and constant k_z to the (degenerate) x and y force constants $k_{x,y}$—to yield oblate ($k_z > k_{x,y}$) and prolate ($k_z < k_{x,y}$) shaped potential wells. Both Upton[39,40] and the present authors[41] have explored the relationship of the spherical jellium model (and its extension to oblate/prolate shapes) to the "crystal field" expansion of the nuclear–electron potential and so clarified the relationship of the jellium model to nuclear configuration. These extensions have extended the scope and removed some of the limitations of the original model, and are discussed in the following section.

B. A Structural Jellium Model

We consider an independent-electron model in which the electron moves in the Coulomb potential of a collection of pointlike atomic cores of effective nuclear charge Z at positions $\mathbf{X}_\alpha$. This potential, $V(\mathbf{r})$, can be expanded in spherical harmonics as follows:[42,43]

$$V(\mathbf{r}) = \sum_{L=0}^{\infty} \sum_{M=-L}^{+L} V_L^M(r,\theta,\phi) \tag{3}$$

where the components of the potential are given by

$$V_L^M(r,\theta,\phi) = \frac{-4\pi Z}{2L+1} \sum_{\alpha=1}^{n} Y_l^M(\theta_\alpha,\phi_\alpha) \left(\frac{r_<^L}{r_>^{L+1}} \right) Y_L^M(\theta,\phi) \tag{4}$$

We employ this expansion just as it is used in crystal field theory:[42] by taking the spherical ($L = 0$) component as the zero-order potential and treating the nonspherical remainder as a perturbation. We use this perturbation, in a qualitative first-order treatment, to evaluate the splitting patterns of each shell (n,l). These splitting patterns enable us to make predictions concerning the shape of both closed-shell and non-closed-shell clusters, while the form of the zero-order potential enables us to suggest necessary conditions for energy level ordering changes, as observed for some mixed clusters.

The matrix elements of a potential component V_L^M are given by the following:[42,44]

$$\langle n,l,m|V_L^M|n',l',m'\rangle = \frac{-4\pi Z}{2L+1} \sum_{\alpha=1}^{n} Y_L^M(\theta_\alpha,\phi_\alpha) \left\langle n,l,m \left| \left(\frac{r_<^L}{r_>^{L+1}} \right) Y_L^M(\theta,\phi) \right| n',l',m' \right\rangle \tag{5}$$

The infinite number of V_L^M components is reduced to a manageable number if we neglect the interaction of states with different principal quantum numbers. Selection rules[42,43] then dictate that only matrix elements of L such that L is even and less than or equal to $2l$ are nonzero and that only values of $M = m - m'$ contribute. Further, once we specify a nuclear geometry, only V_L^M terms that belong to the totally symmetric representation of the point group can contribute to the potential expansion.

The neglect of interaction between states with different principal quantum numbers is a major approximation, as there are no symmetry restrictions on matrix elements of the form $\langle n,l,m|V_L^M|n',l,m\rangle$, which are thus coupled by an infinite number of components of the potential. The major consequence of this is that radial eigenfunctions of the central-field Schrödinger equation, with potential V_0^0, are not good approximations to the actual radial form of the cluster eigenfunctions: the perturbation analysis applies properly only to the *angular* aspects of the problem.

In eq 3, the Coulomb potential $V(\mathbf{r})$ is decomposed into a spherical part, V_0^0, and a nonspherical part. When the former is the major contribution to the potential, we obtain shell structures for clusters with "magic numbers" of electrons. Thus we recapture the essential features of the spherical jellium model if we ingore the nonspherical part of the potential. We note, however, that both the spherical and nonspherical parts of the potential are derived from a well-defined relationship to the Coulomb potential exerted by a particular configuration of atomic cores—hence the name "structural jellium model".[41] The nonspherical part of the potential mixes extensively functions that have the same l and m values (to shift the energy of each shell)

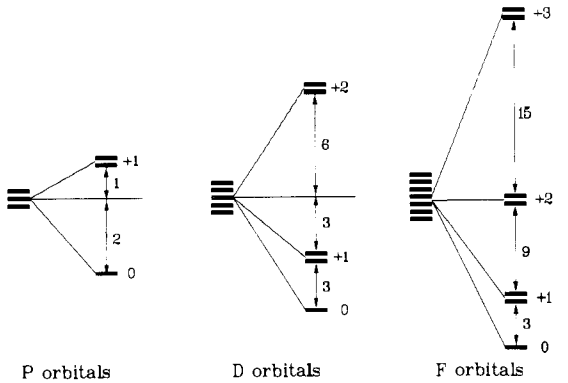

Figure 4. Splitting patterns of shells produced by a V_2^0 perturbation. The sign of the perturbation is such as to yield a prolate-shaped potential well. The splittings obey a barycenter rule so that the sum of all splittings is zero. The individual states are labeled by the z component of their angular momentum.

and, crucially, splits the $(2l + 1)$-fold orbital degeneracy of the shell. This splitting of shells by the nonspherical components of the potential is a determinant of the shape of the cluster for both non-closed-shell and closed-shell electron counts. The splitting is proportional to the effective charge of the atomic cores, tends to decrease (for a given value of l) with increasing nuclearity of the cluster, and tends to increase (for a given nuclearity) with l.[40,41] We now consider how this splitting is determined by, and affects, cluster geometry.

C. The Shape of Non-Closed-Shell Clusters

Very small neutral alkali-metal clusters M_n ($n \leq 8$) have only 1s and 1p solutions of the jellium model filled. The degeneracy of the p shell can be split, but only by the V_2^0 component of the perturbation.[42] We consider a geometry where these n atoms are arranged on a spherical surface of radius r_0. The sign of the splitting is determined by the geometric factor in eq 5; in fact, we can write[41]

$$\text{sign}\,(\Delta E(l,m)) = \text{sign}\,(\sum_\alpha Y_2^0(\theta_\alpha,\phi_\alpha)\langle l,m|Y_L M|l,m\rangle) = \text{sign}\,([\sum_\alpha (3z_\alpha^2 - r_0^2)]\langle l,m|Y_L^M|l,m\rangle) \quad (6)$$

Several standard texts[42,44] show the splitting patterns produced by the matrix elements $\langle l,m|Y_L^M|l,m\rangle$, and these are reproduced in Figure 4 for the case where the geometry-dependent term in square brackets, henceforth abbreviated as $[\sum]$, is positive. In this case the $m = 0$ orbital is of lowest energy, for any l, and the energy increases with $|m|$. This corresponds to a prolate perturbation.

The splittings are governed by a barycenter principle such that the stabilization or destabilization associated with the $p_{\pm 1}$ components is half that associated with p_0.[45] The alternative splitting patterns for oblate and prolate geometries lead directly to a preference for a specific type of distortion as a function of the number of electrons occupying the p shell. In the spherical jellium model stability is associated with the presence of closed shells. Thus an alkali-metal cluster with a total of four electrons, i.e., a $1s^2 1p^2$ configuration, would have a preference for a prolate geometry because the stabilization energy associated with placing two electrons in p_0 is twice as large as that for placing two electrons in $p_{\pm 1}$ (see Figure 4). Similarly, an alkali-metal cluster with six electrons, $1s^2 1p^4$, is oblate. When eight

TABLE 1. Electron Count and Energy for Oblate and Prolate Clusters

electron count	2	3	4	5	6	7	8
oblate	0	β	2β	3β	4β	2β	0
prolate	0	2β	4β	3β	2β	β	0
E(prolate) - E(oblate)	0	β	2β	0	-2β	$-\beta$	0
preferred structure		prolate	prolate		oblate	oblate	

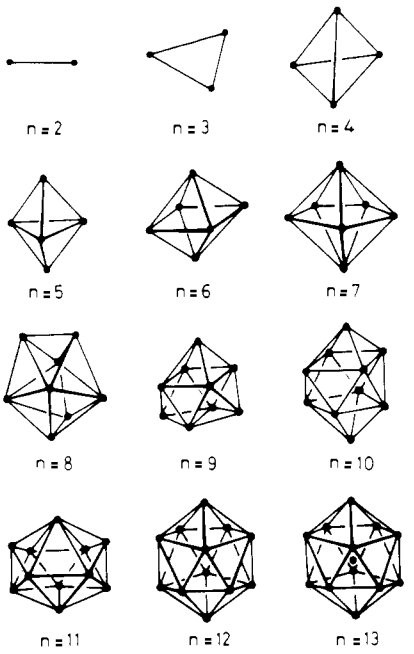

Figure 5. The regular deltahedra. Two points can only define a line; three points are able to define an equilateral triangle. The deltahedra are the tetrahedron (4 points), the trigonal bipyramid (5 points), the octahedron (6 points), the pentagonal bipyramid (7 points), the dodecahedron (8 points), the tricapped trigonal prism (9 points), the bicapped square antiprism (10 points), and the icosahedron (12 points). Eleven vertices cannot define a regular deltahedron, but the closest geometry is shown. Thirteen points characterize a centered icosahedron.

electrons are available, the p shell is completely filled and there is no driving force to reduce the symmetry from spherical. The energy difference between oblate and prolate options is shown as a function of electron count in Table 1.

Oblate and prolate have, of course, strict definitions. A body is oblate (prolate) if the moments of inertia about two orthogonal axes are equal and are greater (less) than that about the third orthogonal axis. The definition we use is based on orbital splittings as defined below. In general, it coincides with the strict definition, but not always, e.g., the edge-shared bi-tetrahedron.

The geometry of a cluster, even with all atoms at the same distance from the center, can be classified as "oblate" or "prolate" according to the sign of $[\sum]$, and this definition is precisely the same as that in terms of the moments of inertia of the clusters. Thus, for example, a trigonal bipyramid is prolate; a pentagonal bipyramid is oblate; a tetrahedron, a cube, or octahedron is spherical ($[\sum] = 0$); a tricapped trigonal prism is oblate; a bicapped square antiprism is prolate; and an icosahedron is spherical. Table 2 classified several common polyhedra as oblate, prolate, or spherical. These polyhedra are shown in Figure 5.

In actual clusters, all nuclei do not generally lie on the same spherical surface. Furthermore, they deviate from this idealized case in such a manner as to enhance their oblate or prolate character. Thus, the equatorial

TABLE 2. Classification of Polyhedra according to Their Oblate/Prolate/Spherical Shape

nuclearity	geometry	shape
4	tetrahedron	spherical
4	square	oblate
5	edge-capped tetrahedron	prolate
5	trigonal bipyramid	prolate
5	square pyramid	oblate
5	pentagon	oblate
6	octahedron	spherical
6	trigonal prism	prolate
6	edge-shared tetrahedra	prolate
6	pentagonal pyramid	oblate
7	capped octahedra	prolate
7	tricapped tetrahedron	oblate
7	pentagonal bipyramid	oblate
8	cube	spherical
8	tetracapped tetrahedron	spherical
8	dodecahedron	prolate
8	square antiprism	oblate
9	capped square antiprism	prolate
9	tricapped trigonal prism	oblate
10	tetracapped octahedron	spherical
10	bicapped square antiprism	prolate
10	pentagonal prism	oblate
10	pentagonal antiprism	oblate
12	icosahedron	spherical

nuclei in the pentagonal bipyramid are farther from the center of the cluster than are the axial nuclei, while the converse is true for the trigonal bipyramid. This occurs because, if the V_2^0 term from a configuration with all nuclei at radius r_0 corresponds to an oblate (prolate) perturbation, then a geometrical distortion of the same oblate (prolate) type will reinforce that perturbation, so increasing the splitting of the p-orbital set.

In summary, the inclusion of a V_2^0 perturbation suggests that non-closed-shell clusters will adopt either an oblate or prolate geometry so as to produce a large HOMO–LUMO gap and hence optimum stabilization of the occupied orbitals. The odd-electron systems are more likely to deviate from the pattern imposed by the structural jellium model with a V_2^0 perturbation.

The arguments developed above not only define the general shape of the cluster but also severely limit the structures that are consistent with this shape. Table 2 provides specific examples of this principle. We shall demonstrate in the next section that these conclusions are very similar to those derived from molecular orbital arguments.

D. An LCAO Model of Shell Structure

The free-electron model has considerably utility in treating the energetics of alkali-metal clusters, and, when combined with ideas from crystal field theory, it can make structural predictions. A complementary approach to structure and bonding in clusters based on an LCAO model[46-48] yields the spherical jellium results for smaller alkali-metal clusters and also enables us to extend the structural predictions to other, seemingly unrelated, clusters.

As in the spherical jellium model, we start with a spherically symmetric model system, but here we restrict ourselves initially to the case of a single shell of atomic cores on the surface of a sphere, so that only the angular aspects of the spherical problem are of concern. The atomic orbital basis functions are categorized as σ, π, or δ type if they have 0, 1, or 2 nodal planes containing the radius vector of the atom, respectively.[46,47]

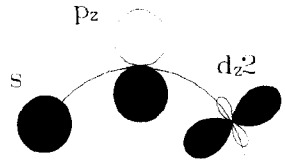

Figure 6. Locally defined s, p_z, and d_{z^2} orbitals, showing their σ character.

Here we consider only σ orbitals,[49-51] returning to the case of π and δ orbitals later.

If we choose a local coordinate system such that the z direction is along the radius vector from the cluster center passing through the atomic core, then the set of σ orbitals includes the s, p_z, and d_{z^2}, orbitals, all cylindrically symmetric about this radius vector. These orbitals are illustrated in Figure 6. Consider first the case where there is only one σ basis function on each atom, which we call σ_α. We then obtain an LCAO wave function from a parent spherical harmonic Y_L^M by setting the coefficient of each atomic orbital equal to the value of Y_L^M at the atom core position:

$$\psi^\sigma_{LM} = \sum_\alpha Y_L^M(\theta_\alpha,\phi_\alpha)\sigma_\alpha$$

where θ_α and ϕ_α are the angular coordinates of atom α.

The conventional shorthand for these symmetry-adapted cluster orbitals is L_M^λ, where $\lambda = \sigma$, π, or δ.[46,47] It is always possible to obtain cluster orbitals L_M^λ that transform according to definite irreducible representations of the molecular point group either by descent in symmetry or projection operator techniques. The approximate spherical symmetry of the clusters suggests that there will be little mixing between L_M^σ of the same point group symmetry but derived from different spherical harmonics: the orthogonality between the parent free-electron wave functions is approximately preserved for the cluster. (The major asymmetry is the concentration of the potential at core sites, and this is accounted for by the use of an LCAO wave function.)

The LCAO wave functions L_M^λ provide a useful framework in which to discuss the closed-shell requirements and structural aspects of ligated clusters. In the general case their approximate energies are best derived from an evaluation of the Coulomb and interatomic resonance integrals rather than from the energy of the parent spherical harmonic.[46] For a cluster where only the valence s orbitals are important for bonding, the two approaches—spherical jellium and LCAO—yield the same energy level pattern.

In Figure 7 the LCAO skeletal molecular orbitals for an icosahedron of s orbitals are illustrated. The most stable molecular orbital is an in-phase combination of all the s orbitals and is designated S^σ, to emphasize the fact that the coefficients of the atomic orbitals have been derived from an expression of the Y_0^0 spherical harmonic. The next most stable set of molecular orbitals is triply degenerate and singly noded, has been derived from Y_1^0, Y_1^1, and Y_1^{-1}, and is described as P^σ. The remaining molecular orbitals have the nodal characteristics of d and f orbitals and are described as D^σ and F^σ. It is noteworthy that only three components of F^σ appear, because the remaining Y_3^M functions are noded at the atom positions.

In general, the L_M^σ set have L nodal surfaces each and so increase in energy with L. The P^σ orbitals only be-

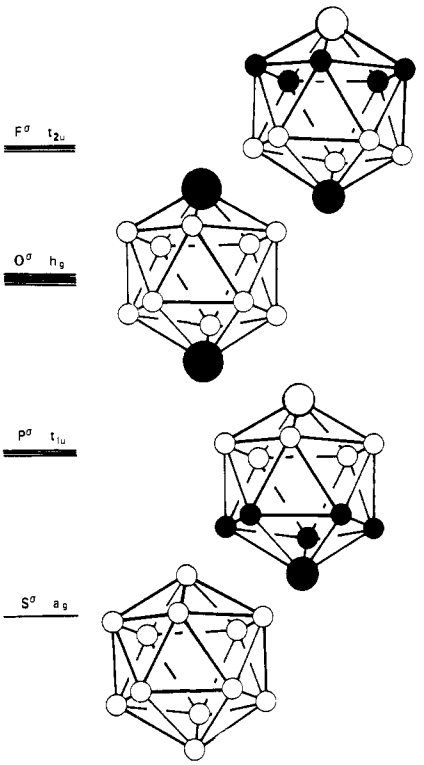

Figure 7. σ molecular orbitals of the icosahedron. In order of increasing energy these molecular orbitals are S^σ (no nodes), P^σ (one angular node), D^σ (two angular nodes)e, and F^σ (three angular nodes). Note that there are only three linearly independent F^σ orbitals.

come overall bonding when $n > 6$, and the D^σ orbitals only become overall bonding when $n > 16$. Further, the splitting patterns of the LCAO $L_M{}^\sigma$ orbitals in the nonspherical case are the same as the splitting pattern of the jellium wave functions shown in Figure 4.

For *small* alkali-metal clusters the LCAO and jellium models give identical conclusions. Clusters with closed shells (at 2, 8, and 18 electrons) will have spherical topologies, should be more stable than adjacent members of the series, and will, in general, have higher ionization potentials.

The energies associated with the S^σ, P^σ, and D^σ shells are determined by the number of nearest-neighbor atoms in the cluster and the nodal properties of the functions. Within a tight-binding or Hückel approximation the stabilization of a molecular orbital depends primarily on the next-neighbor resonance integral terms. For atoms on a singly spherical surface the largest number of nearest neighbors is achieved by deltahedral geometries. A deltahedron has exclusively triangular faces and therefore, by Euler's relationship, the maximum number of edges—or in a chemical context the maximum number of nearest-neighbor interactions. If the atoms lie on several spherical shells, the largest number of nearest-neighbor interactions is achieved by close packing—either in a conventional metallic sense or by icosahedral packing modes with fivefold symmetry.

Therefore, in an LCAO approximation alkali-metal clusters with closed electronic shells—clusters with 2, 8, 18, 20, 34 ... valence electrons—are anticipated to have pseudospherical close-packed structures of high symmetry, i.e., T_d, O_h, or I_h if possible.[52] This conclusion, which has been derived from elementary considerations, is supported by the geometric predictions

TABLE 3. Most Stable Geometries of Lithium Clusters from ab Initio Calculations by Fantucci and Koutecky[a]

molecular formula	electron count	symmetry	structure
Li_3^+	2	C_{2v}	obtuse isosceles triangle
Li_3	3	D_{3h}	equilateral triangle
Li_4^+	3	C_{2v}	triangle, with one terminal atom
Li_4	4	D_{2h}	rhombus
Li_5^+	4	D_{3h}	trigonal bipyramid
Li_5	5	C_{2v}	planar, triangular lattice
Li_6^+	5	D_{2h}	edge-linked tetrahedra
Li_6	6	C_{2v}	pentagonal pyramid
Li_6	6	D_{3h}	planar, triangular lattice
Li_7^+	6	D_{5h}	pentagonal bipyramid
Li_7	7	D_{5h}	pentagonal bipyramid
Li_8^+	7	C_s	capped pentagonal bipyramid
Li_8	8	T_d	tetracapped tetrahedron
Li_9^+	8	D_{4d}	centered square antiprism
Li_9	9	C_{2v}	bicapped pentagonal bipyramid
Li_9	9	C_s	tetracapped trigonal bipyramid
Li_{10}^+	9	C_{2v}	interlinked pentagonal bipyramids
Li_{10}	10	C_{2v}	interlinked pentagonal bipyramids
Li_{14}	14	C_{3v}	
Li_{18}	18	D_{5h}	centered, omnicapped, pentagonal prism
Li_{18}	18	D_{3h}	face-centered cubic
Li_{19}	19	D_{5h}	bi-icosahedron
Li_{19}	19	O_h	centered octahedron
Li_{19}	19	C_{3v}	
Li_{20}	20	T_d	face-centered cubic
Li_{20}	20	T_d	pseudospherical

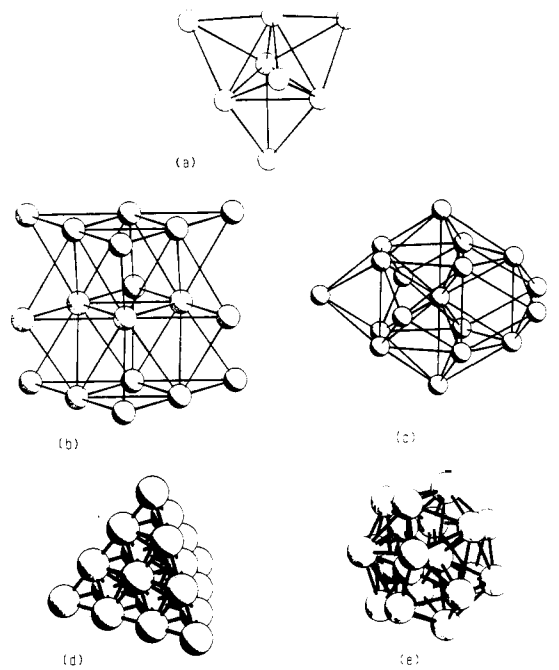

Figure 8. Geometries of neutral alkali-metal clusters with nuclearities and electron counts equal to jellium shell closings, from calculations by Fantucci and Koutecky:[27] (a) Li_8, tetracapped tetrahedron (T_d symmetry); (b) Li_{18}, hexagonal close packed (D_{3h}); (c) Li_{18}, omnicapped pentagonal prism (D_{5h}); (d) Li_{20}, face centered cubic tetrahedron (T_d); (e) Li_{20}, tetrahedron surrounded by points on a spherical surface (T_d).

derived from ab initio calculations by Fantucci and Koutecky,[25,27] listed in Table 3 and illustrated in Figure 8.

It is not possible for all nuclearities to adopt high-symmetry structures. Where a high-symmetry structure can be adopted, this will reinforce the stability associated with a closed electronic shell, whereas if such a structure is not possible, no such reinforcement can occur. Instead, there would be a splitting of the shell

structure, with its attendant instability. We would thus expect the observation of "magic numbers" to depend on the nuclearity of the cluster as well as on the number of electrons. This argument suggests that the magic numbers observed in cation and neutral spectra of the alkali metals may differ: each may exhibit different subsets of the shell-closing numbers predicted by the spherical jellium model.

Neutral sodium clusters exhibit "magic numbers" at n = 8, 20, 40, 58, and 92, but not at n = 18, 34, 68, and 70, which are also closed-shell numbers in the jellium scheme. Although high-symmetry structures (T_d, O_h, or I_h) can be generated for the former set, no such structures exist for the latter. An alkali-metal cation spectrum recently reported showed magic numbers at n = 19, 21, 35, and 41,[30] all numbers for which high-symmetry structures are available (it should be noted that high-symmetry structures are also available for n = 9 and 93). Katakuse et al.[31] have reported discontinuous variations in the ion intensity of mass spectra of gold, sivler, and copper cations at n = 3, 9, 19, 21, 35, 41, 598 93, 139, and 199. LaiHing et al.[53] have carried out laser photoionization experiments on silver cation clusters and report mass spectra with noticeable discontinuities at n = 3, 9, 21, and 41.

It is possible that the absence of large peaks in the spectrum for the "missing" shell-closing numbers is caused not by the absence of high-symmetry structures but by some other factor, such as accidental degeneracies of energy levels or the kinetics of cluster growth, but there is clearly circumstantial evidence in favor of this simple structural jellium model.[52]

It is a well-established principle of molecular orbital theory that molecules with incompletely filled electronic shells undergo distortions in order to increase the energy separation between the highest occupied molecular orbital (HOMO) and the lowest unoccupied molecular orbital (LUMO). Therefore, alkali-metal clusters with incompletely filled P^σ shells are expected to undergo geometric distortions away from the deltahedral geometries preferred by closed-shell molecules. The resultant molecular orbital splitting diagram for olbate and prolate distortions is similar to that described above for a crystal field perturbation and illustrated in Figure 4, except the origins of the splittings are now changes in interatomic resonance integrals arising from changes in internuclear distances. The overall conclusions will, however, be similar to those in Table 1, i.e., prolate geometries preferred for $(S^\sigma)^2(P^\sigma)^2$ and oblate for $(S^\sigma)^2(P^\sigma)^4$. Structures that retain the maximum number of nearest neighbors will, if possible, be retained.

A Hückel molecular orbital study on alkali-metal clusters bears out this conlcuison.[21-23] Hückel calculations on alkali-metal clusters (see Figure 9) pick out, in almost all cases, the most stable cluster structure for cations and neutral clusters, as verified by ab initio calculations, and Hückel calculations on anions[23] are the only available source of information of these species. We consider only species with even numbers of electrons.

Na_3^+ has two electrons (jellium $1s^2$: TSH $(S^\sigma)^2$) and so should be spherical. With only three nuclei, the nearest this cluster can get to spherical is an equilateral triangle, as observed. Meanwhile Na_3^-, with four electrons (jellium $1s^21p^2$), should be prolate, and indeed it

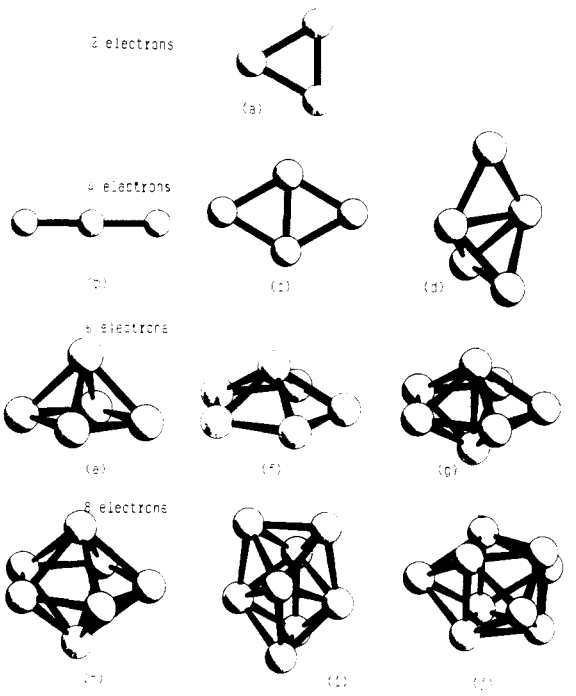

Figure 9. Most stable structures of cationic, neutral, and anionic alkali-metal clusters according to Hückel theory. The geometries obey the predictions of the structural jellium model as far as possible. (a) M_3^+; (b) M_3^-; (c) M_4; (d) M_5^{2-}; (e) M_5^-; (f) M_6; (g) M_7^+; (h) M_7^-; (i) M_8; (j) M_9^+.

is calculated to be linear—an extreme form of prolate geometry.

Na_4^0, with a partially filled 1p shell, adopts a rhomboid shape (strictly speaking, an asymmetric top), which can be viewed as either oblate or prolate, as opposed to a more spherical tetrahedral geometry.

Na_5^+ is an edge-bridged tetrahedron (four electrons; prolate), while Na_5^- is either a square pyramid or a pentagon—they are isoenergetic within the Hückel approximation—both oblate structures.

Na_6^- is a pentagonal pyramid (oblate).

Na_7^+ is an oblate "squashed" pentagonal bipyramid, in which the axial atoms are bonded to one another, while Na_7^- is a pentagonal bipyramid without an axial bond—the closest a seven-atom system can come to a spherical geometry.

Na_8 is a dodecahedron (prolate) in the Hückel approximation, but ab initio calculations show it to be a tetracapped tetrahedron, which is spherical. The adoption of a spherical structure with the atoms on two layers increases the next-nearest-neighbor resonance stabilization energies.

Na_9^+ is a tricapped trigonal prism. Like the pentagonal bipyramid, this is an oblate structure but is as close as a nine-atom structure can come to being spherical.

The simple systems thus obey, in all cases, the dictates of the structural jellium model as far as they can. The odd-electron systems have a smaller energy difference between oblate and prolate forms, and many adopt structures that are neither one nor the other.

The energies of the P levels of several alkali-metal geometries, within the Hückel model, are shown in Figure 10 and show that the anticipated splitting patterns are observed. The tetrahedron has a set of degenerate P orbitals; the prolate trigonal bipyramid exhibits a P_0 orbital below the degenerate $P_{\pm 1}$ pair; the

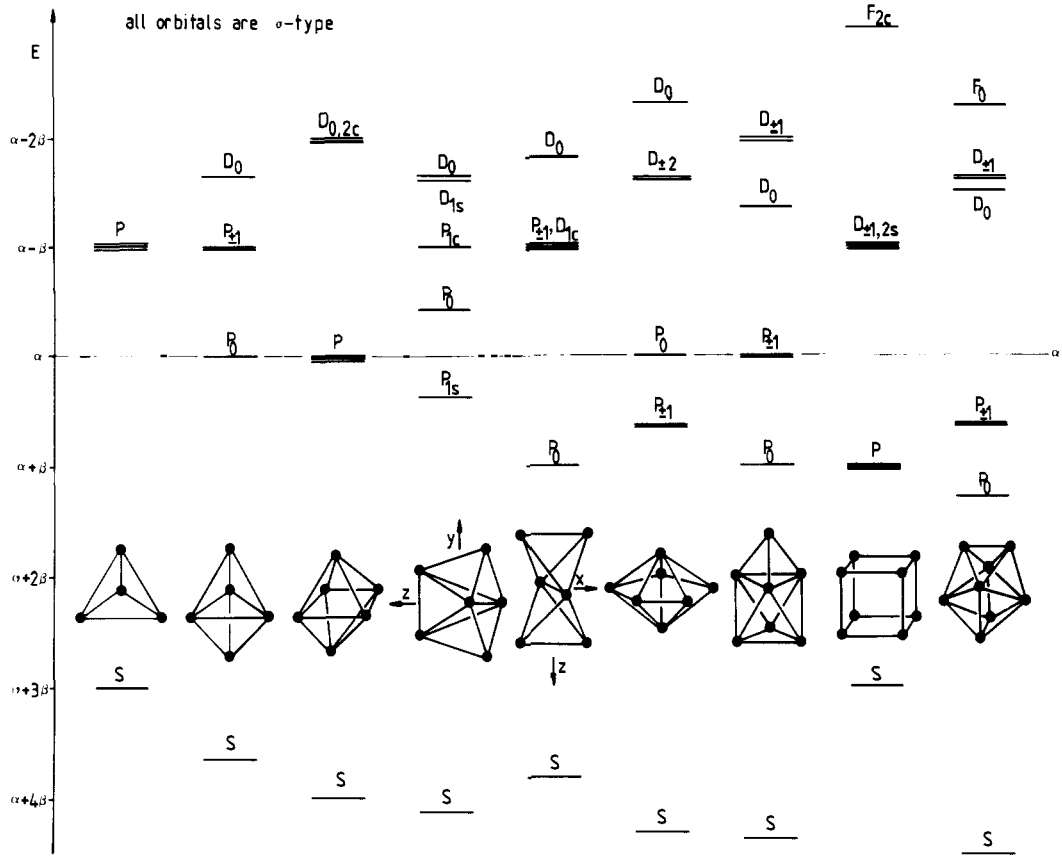

Figure 10. Orbital energies from Hückel theory for small alkali-metal clusters. The orbitals are labeled according to their approximate spherical symmetry. Structures that are spherical, oblate, or prolate give energy orderings as predicted by the structural jellium model.

octahedron again exhibits a degenerate set; the edge-fused tetrahedra of M_8 exhibit the prolate pattern; in the oblate pentagonal bipyramid the ordering is reversed; the capped trigonal prism is prolate; the cube again shows the high degeneracy of spherical systems; and the dodecahedron is prolate.

The fact that, for small clusters at least, the LCAO and jellium approaches give the same predicts concerning the (spheroidal) "shape" of alkali-metal clusters provides an immediate explanation of the, perhaps otherwise surprising, observation that the results of Hückel calculations, called "tight binding" in the context of solid-state physics and applicable principally to insulators,[54] are in accord with the free-electron-based jellium models. Given that these two very different models agree, it is further not surprising that the crude Hückel model gives the right result.

E. Gold Phosphine Clusters and Alkali-Metal Clusters: A Surprising Analogy

An advantage of the LCAO reformulation is that it can be applied to any cluster in which bonding by σ orbitals dominates. An example of such a set of clusters is provided by the ligated gold clusters of formula $[Au_n(PPh_3)_n]^{x+}$ or $[Au(AuPPh_3)_n]^{x+}$.[55] These can be isolated as air-stable crystalline solids and their structures studied in detail by single-crystal X-ray diffraction techniques. The most common ligand observed in gold clusters is PPh_3. Each $AuPPh_3$ fragment in a cluster contributes only one electron for skeletal bonding. The Au–P bond is a dative bond formed from the lone pair of phosphorus and an empty sp hybrid on gold, and the single valence electron of gold is left in an inward-

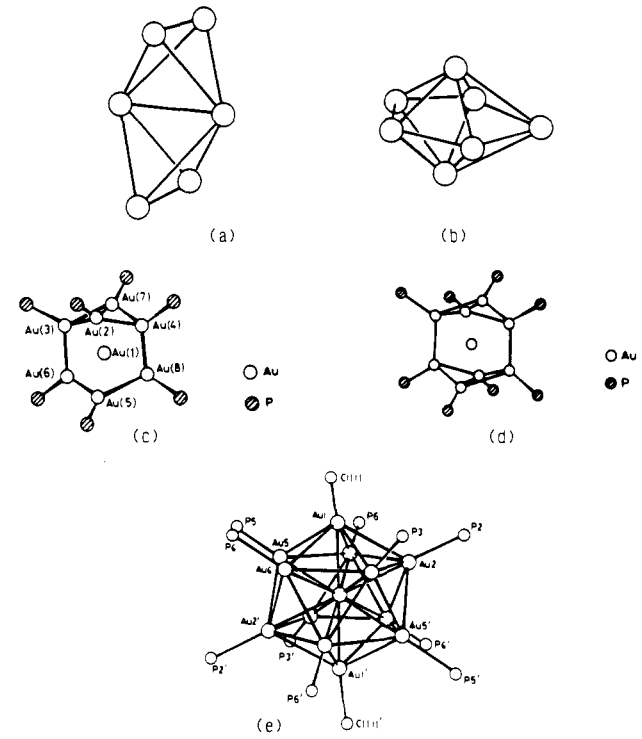

Figure 11. Geometries of gold clusters: (a) $[Au_6(PPh_3)_6]^{2+}$, which adopts a prolate geometry; (b) $[Au_7(PPh_3)_7]^{+}$, which adopts an oblate geometry; (c) $[Au_8(PPh_3)_7]^{2+}$, which adopts an oblate geometry; (d) $[Au_9(P(p\text{-}C_6H_4Me)_3)_8]^{3+}$, which adopts an oblate geometry; (e) $[Au_{13}Cl_2(PR_3)_{10}]^{3+}$, which adopts a spherical geometry.

pointing sp hybrid with a high proportion of s character.[56,57] The gold p_π orbitals are at too high energy to participate significantly in skeleton bonding,[57] and the

gold d^{10} shell is virtually corelike.[57]

The cluster $[Au_6(PPh_3)_6]^{2+}$ has a geometry based on two tetrahedra sharing a common edge.[58] This prolate geometry, illustrated in Figure 11, leads to stabilization of P_0^σ at the expense of the $P_{\pm1}^\sigma$ orbitals, and a closed-shell electron configuration is achieved when the four electrons occupy S^σ and P_0^σ. In contrast, $[Au_7(PPh_3)_7]^+$ has a very distinctive oblate geometry based upon a pentagonal bipyramid with the two axial gold atoms separated by a very short Au–Au bond.[59] In this geometry the P^σ shell splits to give $P_{\pm1}^\sigma$ below P_0^σ and a closed-shell electronic configuration is achieved when these orbitals are fully occupied by six valence electrons. The same geometry has been predicted for Li_7^+ [25] and Na_7^+.[26] Clearly, the alternative symmetrical geometry based on a capped octahedron for $[Au_7(PPh_3)_7]^+$ will not be favored for this electron count since it has a prolate geometry. Moreover, the following electrochemical process should be accompanied by a change in cluster geometry:

$$Au_7(PPh_3)_7^+ - 2e^- \rightarrow Au_7(PPh_3)_7^{3+}$$

oblate pentagonal bipyramid → prolate capped octahedron

Another class of gold clusters is of general formula $[Au_n(PR_3)_m]^{x+}$ and consists of a central gold atom surrounded by $AuPR_3$ moities.[60] The central atom does not alter the electron-counting requirements of spherical, oblate, or prolate geometries, and these clusters too have structures that can be understood in terms of a radial bonding model and hence in terms of an LCAO shell-structure model. Since the central atom has s and p orbitals available for bonding, which overlap strongly with S^σ and P^σ cluster skeletal molecular orbitals, the central atom reinforces the closed-shell requirements of the spherical cluster, a point we return to below. $[Au_{13}Cl_2(PR_3)_{10}]^{3+}$ has eight skeletal electrons and is icosahedral,[61] which is to say spherical. $[Au_6(dppp)_4]^{2+}$, dppp being a bidentate phosphine ligand, has four skeletal electrons and so is predicted to be prolate; it is found to consist of a tetrahedron with two edges bridged,[62] as in Figure 11. $[Au_9(PR_3)_8]^{3+}$ and $[Au_8(PR_3)_7]^{2+}$ are both six-skeletal-electron species, and so are oblate. These geometries, which have also been described as toroidal,[55] are shown in Figure 11.

These results show a very close correspondence in the results for different types of clusters where the primary bonding occurs through radial interactions, and the geometric conclusions could have been derived in either a tensor surface harmonic (TSH) or jellium model, once the separation of ligand and skeletal or cluster bonding electrons is made. This separation is an example of the *isolobal analogy*:[63–65] two cluster fragments are said to be isolobal if they have the same number, symmetry, and approximate energy of valence orbitals and the same number of valence electrons. Hence $Au(PPh_3)$ is isolobal with alkali-metal atoms. Besides recognizing analogies between the gold phosphine and alkali-metal clusters, we also anticipate that clusters of the coinage metals Cu, Ag, and Au would show similar shapes, although there are not the ab initio calculations on such species to check our predictions.

A set of clusters intermediate between the gas-phase bare alkali-metal clusters and the condensed-phase ligated gold clusters is the gas-phase oxidized alkali-metal clusters.[66] The mass spectrum of cesium oxide clusters shows unusually high ionization energies for $Cs_{2n+z}O_n$ (n = 1–7)8, with z = 8, 18, 34, 58, and 92, each of which is a closed-shell number within the jellium scheme. These observations were explained as follows:[66]

"Qualitatively one can think that each oxygen atom bonds two electrons from a sea of delocalized electrons in a Cs cluster. With the use of this picture $Cs_{38}O_2$, $Cs_{40}O_3$, $Cs_{42}O_4$, etc. would be said to contain 34 delocalized electrons. ...Clusters with composition $Cs_{z+2n}O_n$ have z delocalized electrons which can apparently be described as moving in a spherical potential, just as in pure alkali-metal clusters. The orbitals are defined by angular momentum l and the observed anomalies in the mass spectra correspond to electron configurations (1s,1p,1d); (1s,1p,1d,2s,1f); (1s,1p,1d,2s,1f,2p,1g,2d,1h,3s)."

Isolobal gold clusters have been established for lower nuclearity examples with $1s^21p^6$ closed shells,[55,67] e.g., $O(AuPPh_3)_3^+$, $N(AuPPh_3)_4^+$, $[C(AuPPh_3)_5]^+$, and $[C(AuPPh_3)_6]^+$. Otherwise, the structure of these clusters remains unknown, as do the reasons why only certain magic numbers are observed. The clusters are a challenge to both "free-electron" and LCAO approaches in that that separation of what we may call "cluster bonding" electrons from those involved in localized "ligand" bonding arises naturally out of the LCAO approach but not the jellium model, while the large size of these clusters can be accommodated within the jellium model but is currently beyond the scope of LCAO interpretations.

III. Models for Main-Group and Transition-Metal Clusters

Almost 20 years ago, empirical correlations between the structures of cluster compounds and the number of electrons involved in skeletal bonding began to emerge. The contributions of Williams[68,69] and Wade[70,71] were particularly influential in demonstrating that the structures of boranes and carboranes could be related to the parent deltahedral structure that had been elucidated for $B_nH_n^{2-}$. These relationships were extended to the classes of polyhedral molecules by Rudolph,[72] Corbett,[73,74] and Mingos,[75] and the underlying reasons for their success was elucidated by semiempirical molecular orbital calculations.[76] This molecular orbital approach was placed on a more general theoretical foundation by Stone's tensor surface harmonic (TSH) theory.[46–48] A recent review has presented a more detailed historical account of the development of ideas in this area of cluster chemistry.[77] There have been other approaches that have attempted to account for these structural relationships; for example, King[78] has proposed a graph theoretical methodology and Teo[79,80] has developed a topological electron-counting procedure. The discussion below is based on the tensor surface harmonic theory,[46–48] because this model has many similarities to the jellium model developed in the molecular beam area.

A. The Tensor Surface Harmonic Model

We return now to bare clusters and ask when the jellium model is anticipated to break down. The crystal field formulation of the model suggests some criteria

for smallness of the perturbation that is a necessary criterion for the success of the jellium model. Generally speaking, the jellium model fails when the cluster electronic structure can no longer be regarded as a perturbation of a spherical shell model, i.e., when the splitting of the shell produced by the nonspherical part of the potential is large.

The splitting is obviously large for large effective nuclear charges, It has also been shown[40,41] that the splittings are large, for clusters of a given nuclearity, for shells with large angular momentum. These levels are populated when the cluster atoms each have a large number of valence electrons. Further, the splitting of a given shell is expected to decrease for large cluster nuclearities. Thus we can conclude that the jellium model will fail for clusters with a large number of valence electrons per atom, and for small clusters in particular. Clearly, we cannot expect the jellium model to apply properly to p-block elements (with the possible exception of aluminum) or to transition metals, with the exception of the coinage metals, for which it works reasonably well.

The LCAO approach illuminates the reasons for failure of the jellium model, but from a different perspective. Many main-group and transition-metal ligated clusters can be treated as having approximate spherical symmetry, as mentioned above. They will therefore exhibit some form of shell structure—characteristic sets of quasi-degenerate orbitals. A proper LCAO treatment of this situation, including not only the $L_M{}^{\sigma}$ orbitals described above but also $L_M{}^{\lambda}$ orbitals of π and δ type, has been carried out by Stone and is called by him tensor surface hamonic theory.[46-48] It reveals that the basic features of the electronic structure of main-group and transition-metal ligated clusters are different from those of the free-electron metals. The results of this analysis are summarized briefly below. References 46–48 provide a more detailed description of the methodology.

We look here at the π orbitals, important for main-group clusters. We can form cluster orbitals from the π basis orbitals (local p_x and p_y orbitals) if we exploit the fact that they behave locally like a pair of orthogonal vectors tangential to the surface of the sphere. If we can find a *vector* function of θ and ϕ, then the direction and magnitude of the vector at $(\theta_\alpha,\phi_\alpha)$ will indicate the direction and magnitude of a π-orbital contribution to a cluster wave function.

We can form two such vector functions from the spherical harmonics (except for $L = M = 0$). The first is given by the gradient of the spherical harmonic:

$$\mathbf{V}_{LM} = \nabla Y_L{}^M(\theta,\phi) \tag{7}$$

and the second by

$$\bar{\mathbf{V}}_{LM} = \mathbf{r} \wedge \nabla Y_L{}^M(\theta,\phi) \tag{8}$$

the cross product of the position vector with the gradient of the spherical harmonic.

These two *vector surface harmonics* are shown in Figure 12. They are at right angles to each other at every point on the sphere, Figure 13 shows how the P^{π}, D^{π}, $\bar{P}^{\pi}$, and $\bar{D}^{\pi}$ molecular orbitals of the octahedron are derived from the vector spherical harmonics $\mathbf{V}_{1M}$, $\mathbf{V}_{2M}$, $\bar{\mathbf{V}}_{1M}$, and $\bar{\mathbf{V}}_{2M}$, respectively.

It can be seen that the $\bar{L}^{\pi}$ orbital derived from $\bar{\mathbf{V}}_{LM}$ can be constructed from the corresponding L^{π} orbital

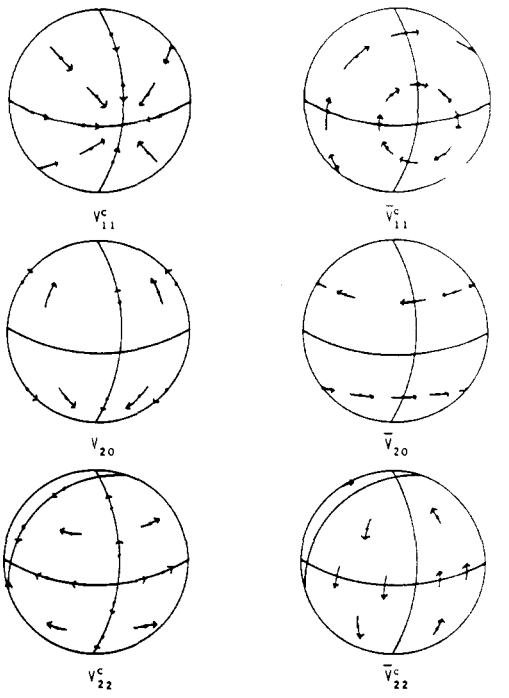

Figure 12. Vector surface harmonics on a sphere, with the direction and magnitude of the vector function at selected points indicated by arrows. The functions V_{lm} are formed by taking the gradient of the spherical harmonic Y_{lm}, while the functions $\bar{V}_{lm}$ are formed by taking the cross product of the position vector with the function V_{lm}. The superscript "c" indicates that the cosine combination of functions Y_{lm} and $Y_{l,-m}$ have been taken.

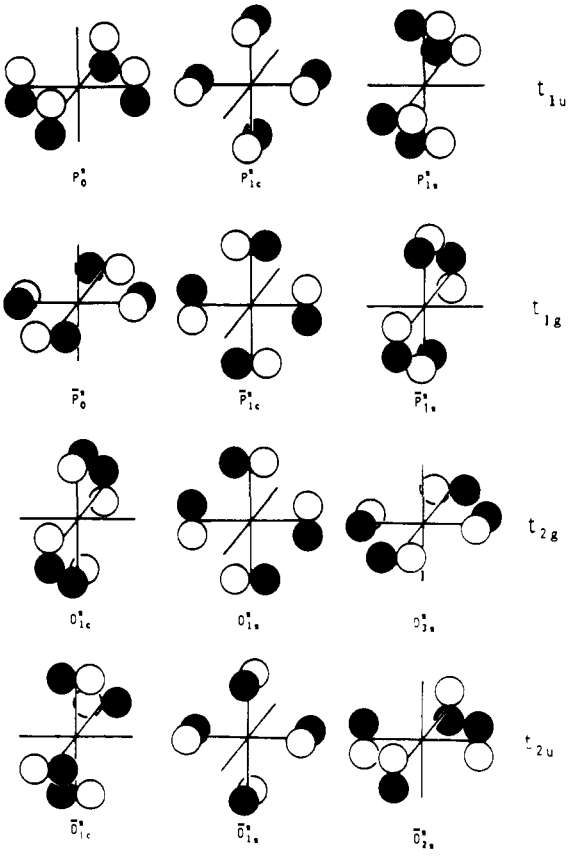

Figure 13. The π orbitals of the octahedron, with their TSH classification and point group symmetry classification.

by rotating every atomic π function through 90°. This is a general result. Further, the rotation converts a bonding interaction between two orbitals into an antibonding interaction, and so a pairing theorem can be

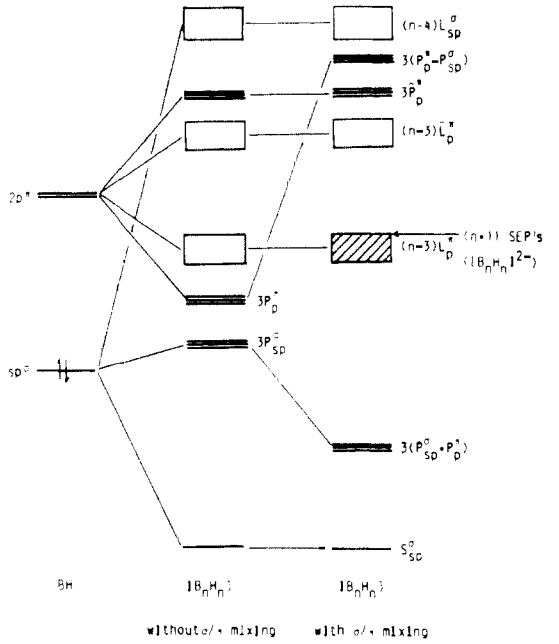

Figure 14. Interaction among σ and π orbitals of borane deltahedra leading to the resulting energy levels of the deltahedron on the right.

shown to hold for the cluster π orbitals. The orbitals constructed from $\mathbf{V}_{LM}$ are bonding, and those constructed from $\bar{\mathbf{V}}_{LM}$ antibonding for deltahedra.[46,47]

As a result of this pairing theorem, the $2n$ p orbitals of π symmetry yield n bonding orbitals and n antibonding orbitals for any polyhedron. A Hückel approach, and inspection of Figure 13 for the special case of the octahedron, show that the highest value of L generated by the cluster under consideration will yield the *lowest* energy L^{π} orbitals. thus for an octahedron we will find six accessible L^{π} orbitals: three D^{π} orbitals and, at higher energy, three P^{π} orbitals. These are illustrated in Figure 13.

The differing behavior under inversion of the bonding and antibonding orbitals limits the orbital mixing that can occur in clusters. The L^{σ} and L^{π} orbitals of the same L and M values can mix with each other, but there is not mixing with $\bar{L}^{\pi}$ orbitals.

We have already shown that for most main-group clusters the L^{σ} orbitals will be antibonding for all but the S^{σ} while there will generally be n π bonding orbitals. The L^{σ} and L^{π} orbitals, where they can mix, will interact to produce one bonding and one antibonding combination. This interaction does not alter the total number of bonding orbitals, although it can and does alter the energy level ordering among the bonding orbitals. Figure 14 shows, again for the octahedron, how the interactions among the orbitals is restricted by symmetry and how the interactions that do take place alter the energy ordering of the bonding manifold but, crucially, do not alter the *number* of bonding orbitals. In summary, the total number of bonding orbitals for a deltahedron will thus be $n + 1$.

The full development of tensor surface harmonic theory is not given here. Instead, we simply summarize the electron-counting rules that have been deduced from tensor surface harmonic theory together with the use of the isolobal analogy and molecular orbital calculations. This complex of ideas together with the rules deduced from them goes under the name "polyhedral skeletal electron pair theory" (PSEPT).

TABLE 4. Closed-Shell Requirements for Ligated Main-Group and Transition-Metal Clusters with n Atoms

structure	main-group cluster	transition-metal carbonyl cluster
deltahedral		
closo	$4n + 2$ electrons	$14n + 2$ electrons
nido	$4n + 4$ electrons	$14n + 4$ electrons
arachno	$4n + 6$ electrons	$14n + 4$ electrons
hypho	$4n + 8$ electrons	$14n + 8$ electrons
three-connected		
closo	$5n/2$ electrons	$15n/2$ electrons

B. Polyhedral Skeletal Electron Pair Theory

Electron-Counting Rules for Main-Group Ligated Clusters

The LCAO approach briefly summarized above provides a powerful framework for rationalizing the geometries and closed-shell requirements of main-group clusters. In particular, there is an intimate relationship between the polyhedral geometry and the number of valence electrons required for achieving an electronic closed shell and a large HOMO–LUMO gap. The pioneering molecular orbital studies on $B_nH_n^{2-}$ by Longuet-Higgins[49] and Lipscomb and Hoffmann[51] were important in highlighting these relationships, although it was Williams[69] and Wade[71] who proposed the specific relationship between the geometric and electronic aspects of the structures. In deltahedral clusters the bonding is highly delocalized, and the nodal patterns associated with the molecular orbitals are accurately represented by the tensor surface harmonic theory. With a slight oversimplification, it can be stated as above that in such molecules there are n L^{π} tangential bonding skeletal molecular orbitals derived from p_{π} orbitals, and a single radial S^{σ} molecular orbital, i.e., $n + 1$ skeletal bonding molecular orbitals. These molecules have a further n out-pointing radial molecular orbitals which are not used for skeletal bonding but are available either for electron-pair occupation ("lone pairs") or for forming σ bonds to ligating atoms, such as H, Cl, or CH_3. Therefore, such deltahedral clusters are characterized by a total of $2n + 1$ available molecular orbitals, which can accommodate a total of $4n + 2$ valence electrons.

This bonding pattern is retained even in those deltahedral molecules that have 1–3 atoms missing. Such molecules are described as nido ($n - 1$), arachno ($n - 2$), and hypho ($n - 3$) to distinguish them from the parent deltahedron, which is described as closo. These incomplete polyhedral fragments retain the $n + 1$ skeletal bonding molecular orbitals of the parent deltahedron[71] but of course no longer have the electron pairs associated with the B–H σ-bonding and out-pointing orbitals of the missing vertices. The resulting closed-shell requirements of these molecules are summarized in Table 4. Examples of polyhedral boranes showing these relationships are illustrated in Figure 15.

In three-connected main-group polyhedral molecules the bonding can adequately be described in terms of localized two-center, two-electron bonds along the edges, and the large and clear separation between L^{π} and $\bar{L}^{\pi}$ tangential skeletal molecular orbitals is no longer observed. Since three-connected polyhedra have a total of $3n/2$ edges, such molecules are characterized by $3n/2$

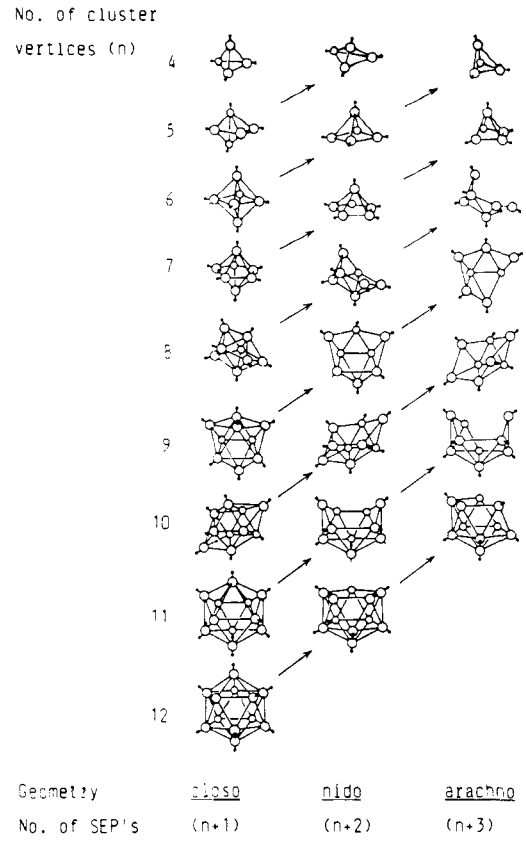

Figure 15. Polyhedral borane structure, showing the relationship between the number of cluster vertices and skeletal electron pair count. Adapted from: Rudolph, R. W.; Pretzer, W. R. *Inorg. Chem.* **1972**, *11*, 1974.

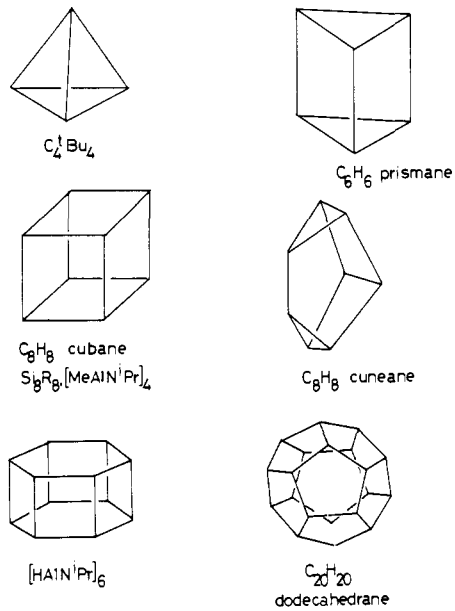

Figure 16. Structures of three-connected compounds, of which hydrocarbons form a major subset.

skeletal bonding molecular orbitals, and n out-pointing bonding molecular orbitals, which can be used to accommodate "lone pairs" or for bonding to ligands. The hydrocarbons provide the most extensive series of three-connected polyhedral molecules, and some of their structures are illustrated in Figure 16. Interestingly, P_4 provides an inorganic example of a three-connected (tetrahedral) cluster belonging to this class.

The polyhedral skeletal electron pair theory summarized briefly above has been successfully applied to boranes, hydrocarbons, carboranes, heteroboranes, anionic "naked" clusters of tin, germanium, and lead, cationic "naked" clusters of bismuth, and ring compounds of the later main-group elements.[81,82]

TABLE 5. Isostructural Main-Group and Transition-Metal Clusters

structure	main-group cluster	electron count	transition-metal carbonyl cluster	electron count
trigonal bipyramid	$C_2B_3H_5$	22	$Os_5(CO)_{16}$	72
square pyramid	B_5H_9	24	$Ru_5C(CO)_{15}$	74
octahedron	$C_2B_4H_8$	26	$Os_6(CO)_{18}^{2-}$	86
pentagonal bipyramid	$C_2B_5H_7$	30		
tricapped trigonal prism	$C_2B_7H_9$	38		
bicapped square antiprism	$C_2B_8H_{10}$	42	$Rh_{10}S(CO)_{22}$	142

Naked clusters are those that do not require ligands to stabilize them, e.g., Sn_9^{4-} and Bi_9^{5+}, and therefore most closely resemble clusters in molecular beams. These condensed-phase clusters go under the name of Zintl clusters.[73,74] PSEPT is therefore a theory with wide applicability, few exceptions, and a firm theoretical foundation. In the subsequent section we shall demonstrate its applicability to main-group clusters in molecular beams.

Closed-Shell Requirements for Transition-Metal Carbonyl Clusters

The spectrum of molecular orbitals generated from s and p atomic orbitals described above is also relevant to transition-metal carbonyl clusters. In particular, isostructural main-group and transition-metal carbonyl clusters generate closely related sets of radial and tangential bonding skeletal molecular orbitals. Although the five d orbitals per metal atom play an important metal–metal bonding role, they make a secondary contribution to defining the electronic requirements of the cluster. In consequence, the number of available orbitals in isostructural closo main-group and transition-metal clusters differs by $5n$, where n is the number of skeletal metal atoms. Table 5 provides some specific examples. Some examples of deltahedral and three-connected transition-metal carbonyl clusters that conform to this generalization are illustrated in Figure 17.

In addition to these polyhedra, transition-metal carbonyl clusters are noted for their ability to form families of capped structures. Many hundred of these capped structures have now been characterized,[83] and a typical illustrative series is shown in Figure 18.[84] Some years ago we defined the consequences of these capping processes on the closed-shell requirements of the parent polyhedral entity and demonstrated that such capped structures are usually associated with an increment in the total valence electron count of 12.[85,86] The series illustrated in Figure 18 provide a specific illustration of this principle.

IV. Applications of PSEPT to Clusters in Molecular Beams

A. PSEPT Applied to Gas-Phase Main-Group Clusters

During the last 5 years, laser vaporization and cluster beam techniques have been extended to main-group elements and compounds,[87] the elements involved in the

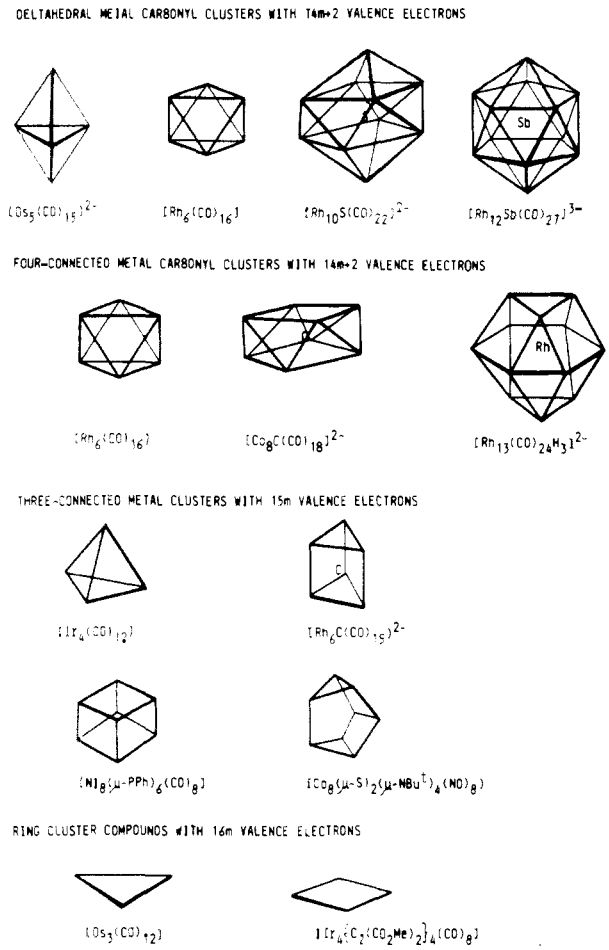

Figure 17. Deltahedral, four-connected, three-connected, and ring transition-metal carbonyl clusters, with their electron counts. This illustrates the range of structures that can be encompasses within the PSEPT approach.

semiconductor industry having been the subject of particularly intense study.[88] A substantial body of results concerning the stability, ionization potentials, reactivity, and fragmentation behavior of main-group clusters now exists, but understanding of the stability trends and knowledge of cluster structures are in their early stages. The structure and stability of main-group clusters, both elemental and compound, are intrinsically more complicated than those of the alkali metals and noble gases. In order to understand the stability trends of these clusters, a knowledge of the structural possibilities open to all members of a series is required, so that the energies of each cluster can be compared.

A large and interesting class of main-group clusters has close to $4n$ valence electron, and investigation of the structural possibilities open to these clusters can be substantially simplified by use of PSEPT. We discuss the structures of this class of main-group clsuters here. The applicability of PSEPT to these situations has also been alluded to in specific cases by Martin,[89,90] Duncan and co-workers,[91,92] and Schild et al.[93] We present evidence below that its applicability is widespread. Our findings differ from models proposed by some other workers, based on analogies with solid-state structures and arguments concerning coordination numbers. Indeed, the sparsity of structural information combined with the rapid growth of interst in these clusters has led to many speculations concerning structural possibilities for main-group clusters, several of which can be

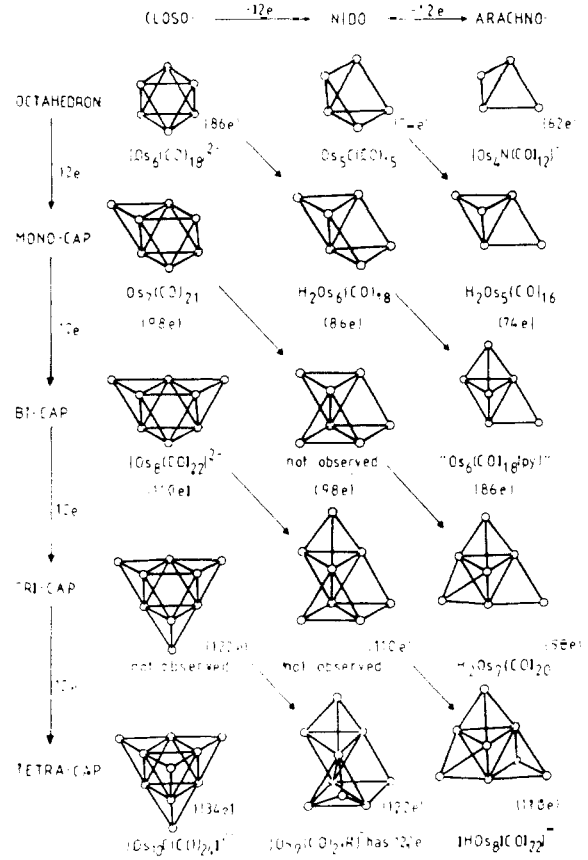

Figure 18. Capped osmium clusters, with their valence electron counts. These clusters show how capping and the forming of nido and arachno structures, when combined, can lead to a wide variety of known structures with well-defined electron counts.

discounted when the restrictions imposed by PSEPT are applied to the problem.

Gas-Phase Zintl Clusters

The utility of PSEPT electron-counting rules in understanding the stabilities of main-group clusters was first pointed out by Martin[69] and by Duncan et al.[91] in studies of compound clusters of group 14 and group 15 metals, clusters that have also been investigated by Schild et al.[93]

Martin[89] has observed compound gas-phase clusters by cocondensing cesium with the group 14 metals Sn and Pb. The Zintl species $Cs_3Pb_5^+$, $Cs_3Sn_5^+$, $Cs_3Sn_9^+$, and $Cs_5Sn_9^+$ appear to be particularly stable (Martin's apparatus was not able to measure peaks up to the mass of $Cs_3Pb_9^+$ or $Cs_3Pb_9^+$), and Martin suggested that, by analogy with the solid-state structures, these species would have deltahedral frameworks for the group 14 element: $Cs_3M_5^+$ a trigonal bipyramid, $Cs_3Sn_9^+$ a tricapped trigonal prism, and $Cs_5Sn_9^+$ a capped square antiprism (a *nido*-deltahedron). These clusters are isoelectronic with the Zintl ions studied in the solid and liquid state,[73,74] such as Sn_5^{2-}, Pb_5^{2-}, Pb_9^{4-}, Bi_9^{5+}, and Ge_9^{4-}, and as the electron-counting rules are known to work for these ligand-free ions in condensed-phase chemistry,[73,94] the deltahedral structures are obvious candidates for the structures of the gas-phase analogues. The trigonal bipyramid (Sn_5^{2-}), tricapped trigonal prism (Bi_9^{5+}), and capped square antiprism (Pb_9^{4-}) are shown in Figure 19. To the $(2n + 2)$ skeletal bonding electrons that characterize the *closo*-deltahedral must be added n radical nonbonding orbitals, containing either "lone

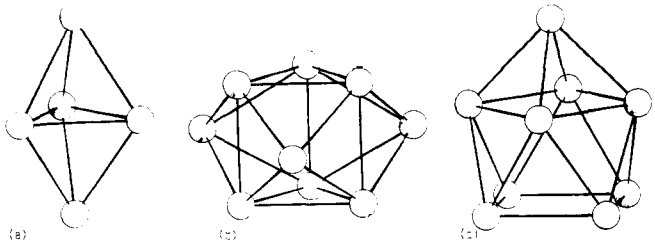

Figure 19. Structures of bare clusters of main-group elements: (a) trigonal bipyramid, adopted by Sn_5^{2-}; (b) tricapped trigonal prism, adopted by Ge_9^{2-}; (c) capped square antiprism, adopted by Pb_9^{4-}.

pairs" or "corelike" s orbitals (depending on the element), giving a total of $(4n + 2)$ valence electrons. The polyanion Sn_9^{2-} has not been observed, but Ge_9^{2-} has been observed in the solid state as a tricapped trigonal prism.[95] $Cs_5Sn_4^+$ was also observed to be particularly stable among the $Cs_5Sn_n^+$ series, along with $Cs_5Sn_9^+$, and a tetrahedral structure was suggested, by analogy with the isoelectronic P_4.

In a previous section we noted that alkali metals are *isolobal* with $AuPR_3$, and this connection provides some additional information concerning the structures of these clusters. The $AuPR_3$ fragment is able either to cap or, if steric requirements do not permit it, to edge-bridge deltahedral clusters without changing their basic geometries or electron counts. We propose that in these cesium clusters the Cs^+ ions are face-capping unless the number of faces of the group 14 deltahedron is exceeded.

Mass spectra of group 14/group 15 compound clusters produced by cocondensation were observed by Schild and co-workers[93] as well as by Duncan and co-workers.[91,92] These spectra showed highly nonstatistical distributions, being dominated by the following species: $Sn_2Bi_3^+$, $Pb_2Sb_3^+$, $Sn_2As_3^+$, $Pb_2As_3^+$ and $Sn_4Bi_5^+$, $Pb_4Sb_5^+$, $Sn_4As_5^+$, $Pb_4As_5^+$ (in conditions under which the spectrum could be interpreted in terms of cation stabilty); and Sn_3Bi_2, Pb_3Sb_2, Sn_3As_2, Pb_3As_2 and Sn_5Bi_4, Pb_5Sb_4, Sn_5As_4, Pb_5As_4 (under neutral conditions). These five- and nine-atom clusters are isoelectronic with the Zintl polyanions observed by Martin[89] and are likely to be isostructural also, having trigonal-bipyramidal and capped square-antiprismatic geometries, respectively.

Other species were observed in these spectra by Duncan and co-workers,[91,92] although at lower intensity than the five- and nine-atom clusters. Examples include Pb_4Sb_2, Sn_4As_2, $Sn_3Bi_3^+$, $Pb_3Sb_3^+$ (all with six atoms and twenty-six valence electrons); Pb_5Sb_2, $Sn_4Bi_3^+$, $Sn_4As_3^+$ (seven atoms, thirty valence electrons); and Pb_6Sb_4, Sn_6As_4, $Sn_5Bi_5^+$ (ten atoms, forty-four electrons). These may thus be assigned *closo*-deltahedral structures, save the last set, which have the nido electron count.

The spectra of the group 13/group 15 compound clusters In_xBi_y and In_xSb_y have also been observed by Duncan and co-workers.[96] In addition to species with $4n$ valence electrons, which are discussed below, several $(4n + 2)$-electron species were observed in significant abundance. $InSb_4^+$ and $InBi_4^+$ are the predominant species in the cation spectra of these systems, are isoelectronic with Zintl species, and so are expected to be trigonal bipyramidal. Also observed in the cation spectra were $In_2Bi_5^+$ and (to a lesser extent) $In_2Sb_5^+$, which are expected to be pentagonal bipyramidal, and In_2Bi_4 and (to a lesser extent) In_2Sb_4, which are predicted to be octahedral within the PSEPT scheme.

TABLE 6. Valence Electron Counts and Predicted Structures of Gas-Phase "Zintl" Clusters

atom and electron count	predicted structure	examples
4, 20	tetrahedron	As_4, Sb_4, Bi_4, Sn_4^{4-}
5, 22	trigonal bipyramid	Sn_5^{2-}, Pb_5^{2-}, $Sn_2Bi_3^+$, $Pb_2Sb_3^+$, $Sn_2As_3^+$, $Pb_2As_3^+$, Sn_3Bi_2, Pb_3Sb_2, Sn_3As_2, Pb_3As_2, $InSb_4^+$, $InBi_4^+$
6, 26	octahedron	$Sn_3Bi_3^+$, $Pb_3Sb_3^+$, Pb_4Sb_2, Sn_4As_2, In_2Sb_4, In_2Bi_4
7, 30	pentagonal bipyramid	$Sn_4As_3^+$, $Sn_4Bi_3^+$, Pb_5Sb_2, $In_2Sb_5^+$, $In_2Bi_5^+$
9, 38	tricapped trigonal prism	Sn_9^{2-}
9, 40	capped square antiprism	Sn_9^{4-}, $Sn_4Bi_5^+$, $Sn_4As_5^+$, $Pb_4Sb_5^+$, $Pb_4As_5^+$, Sn_5Bi_4, Pb_5Sb_4, Sn_5As_4, Pb_5As_4
10, 44	nido 11-vertex deltahedron	$Sn_5Bi_5^+$, Sn_6As_4, Pb_6Sb_4

Table 6 summarizes many of these structural conclusions drawn from PSEPT arguments.

Clusters of Group 14 Elements and Semiconducting Elements

The $(4n + 2)$-electron clusters are direct analogues of known "bare clusters" that exist in condensed phases. Many other gas-phase clusters have $4n$ valence electrons: examples of particular importance are the group 14 elements as well as some of the species seen in concondensation experiments of group 13 and group 15 elements. The closeness of the electron count to the values required for deltahedra suggests that deltahedra-based geometries are possible for these clusters. They are faced, however, with the necessity of removing one orbital from the bonding manifold compared to the closo structure.

PSEPT suggests two methods for the destabilization of this orbital for small clusters. One is to cap a smaller deltahedron: the capping principle developed for ligated clusters tells us that capping a polyhedron adds no orbitals to the skeleton bonding manifold, so with the "lone pair" adding a single orbital, a capped deltahedron composed of a total of n atoms is characterized by $(2(n - 1) + 1) + 1 = 2n$ orbitals. In addition to these, clusters with three or more caps can also include extra orbitals in the bonding manifold[97] as they approach the bispherical case, with a central core of cluster atoms surrounded by an outer spherical shell of cluster atoms. A second possibility for small clusters that has no analogue in ligated clusters is the distortion of a pseudospherical cluster by a "squashing" mode along the principal axis to form an oblate shape. This distortion removes one orbital of p symmetry that is antibonding along the principal axis by "pushing" it to higher energy. These two possibilities may lead to several, just one, or no "electron-correct" structures for each cluster. The possibilities generated by this approach for nuclearities four to ten are as follows:[98] Si_4, rhombohedral; Si_5, oblate trigonal pyramid; Si_6, bicapped tetrahedron or oblate-distorted octahedron; Si_7, oblate pentagonal bipyramid, capped octahedron, or tricapped tetrahedron; Si_8, capped pentagonal bipyramid; Si_9, capped dodecahedron; Si_{10}, tetracapped trigonal prism or tetracapped octahedron.

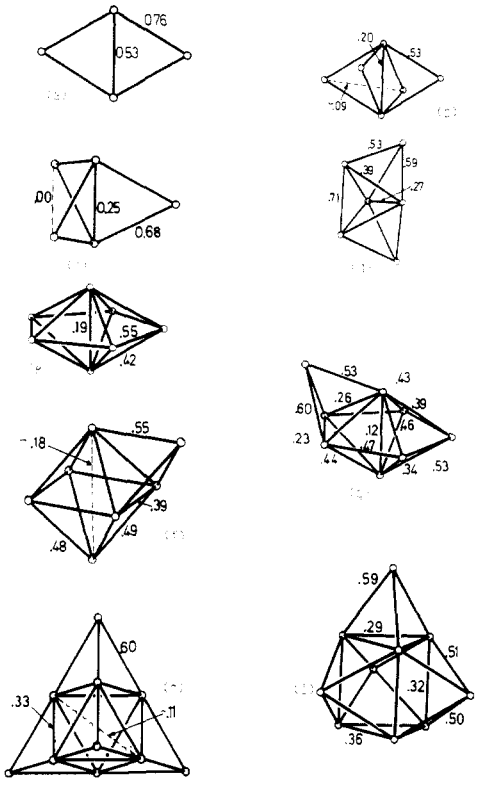

Figure 20. Electron-correct structures for small silicon clusters. The numbers by each bond show the overlap populations from extended-Hückel calculations and indicate the relative bond strengths within the cluster. Some cluster nuclearities have several possible electron-correct structures. (a) Si_4, rhombus; (b) Si_6, oblate-distorted octahedron; (c) Si_5, oblate trigonal bipyramid; (d) Si_6, bicapped tetrahedron; (e) Si_7, oblate pentagonal bipyramid; (f) Si_7, capped octahedron; (g) Si_8, capped pentagonal bipyramid; (h) Si_{10}, tetracapped octahedron; (i) Si_{10}, tetracapped trigonal prism.

These structures are shown in Figure 20. The silicon clusters of nuclearity up to ten have been the subject of more computational studies than any other main-group cluster system. The most accurate and comprehensive calculations to data are those by Raghavachari and co-workers.[99-101] These studies show that *all* of the above structures investigated correspond to minima on the potential energy surface and that the global minimum is, in all cases but Si_8 and Si_9 (for which the capped dodecahedron has not been investigated), one of these electron-correct structures: the capped pentagonal bipyramid for Si_8 is unstable because of the short axial Si–Si distance. It is interesting to note that many of these structures are analogous to structures of ligated osmium clusters.[84]

The mass spectra of silicon and germanium clusters have been observed under a wide variety of conditions:[102-104] laser photoionization mass spectra have been taken under high laser power conditions that yield information on the cations as well as low-power conditions that yield information on the neutral species.[104] Electron impact ionization mass spectra have also been observed, and fragmentation patterns studied. The results are not all consistent with each other but, taken together, do indicate that cation or neutral species with six, seven, or ten atoms seem particularly stable for Si and Ge clusters. The six- and ten-nuclearity species are the only ones for which polycapped structures are possible, suggesting that there is a stability associated with capping. Together with the considerabl stability of M_7, this suggests a general rule that silicon and germanium clusters that can form an electron-correct structure by capping or by oblate distortion without the loss of significant equatorial bonding will be particularly stable.

Phillips has suggested that the particular stability of the Si_{10} cluster is associated with a fragment of the crystal "adamantane" lattice,[105,106] but calculations have shown this structure to be considerably less stable than the more densely packed capped-trigonal-prism and capped-octahedron structures.[101] Although interpretations of these structures have been offered in terms of average coordination number and hybridization patterns, neither of these approaches has the breadth of scope of the PSEPT approach.

Molecular dynamics studies[107] lead to structures that can often be ruled out by PSEPT. The ground-state structure predicted for Si_6 is the trigonal prism, which we have shown to be electron incorrect; they predict Si_7 to adopt the tetracapped-tetrahedron geometry, which is electron correct, while they predict another three-connected structure, the cube, for the ground-state geometry of Si_8.

Calculations based on nonspherical interatomic potentials[108] produce structures that are too open for small silicon clusters, being based on five- and six-membered rings, far more similar in behavior to carbon clusters.

There is a marked difference in the mass spectra of silicon and germanium cluters from those of tin and, particularly, lead.[109] Although all these elements show similar beahavior in the region $n \leq 10$, lead shows a "magic number" at a nuclearity of thirteen, and tin shows some evidence of stability at this nuclearity also. This has been associated with a centered icosahedral geometry.[106] This result can be explained simply within the PSEPT scheme, which suggests that this geometry may indeed be stable for lead, but not for silicon. The relative energy of the valence s and p orbitals makes no difference to the electron-counting rules for clusters with no interstitial atoms. With the appearance of interstitial atoms, however, the energy of the s orbital may become important for electron-counting purposes.

If the s orbitals are included in the valence shell, the antibonding combination of the interstitial s orbital and the S function of the deltahedron will be of high energy. The centered icosahedron will thus be characterized by $(4n - 2) = 50$ valence electrons, and this geometry would be unstable for an element with a high-energy s orbital. If the s orbital can be treated as a core orbital, then all n linear combinations of s orbitals will be occupied, and the cluster will be characterized by $4n$ (including s orbitals) or $2n$ valence electrons (neglecting s). Thus, Pb_{13} is expected to be more stable in the centered icosahedral geometry than Si_{13}. No calculations have yet been carried out to check this suggestion. The high coordination of this cluster is a reflection, in cluster chemistry, of the same characteristics that make lead a close-packed metal while silicon and germanium are "network-bonded" crystals. PSEPT also suggests that Pb_{19} should be an octahedron with one interstitial atom rather than the icosahedrally based structure with two interstitial atoms suggested by Phillips.[106]

Phillips[105,106] has proposed that the magic nubmer of lead can be understood if both packing and jellium closed shells are considered. Noble gas clusters have

stabilities determined by favorable packing arrangements, the sequence of icosahedral structures with n = 13, 55, etc. being particularly stable.[5,110] Phillips suggests that the magic numbers at n = 7, 13, and 19 in the lead mass spectrum may be interpreted in terms of close-packed structures with fivefold symmetry (the pentagonal bipyramid, the centered icosahedron, and the "bi-icosahedron"), while that at n = 10, with 40 electrons, could be interpreted in terms of a jellium closed shell. Phillips suggests a bicapped square antiprism for this n = 10 isomer. We have seen in the discussion above that this closo structure will be characterized by 42 electrons, and so is not a likely candidate for the Pb_{10} structure. The structure is more likely to be an analogue of the Si_{10} structure above. It should be noted, however, that ultraviolet photoelectron spectroscopy experiments on silicon and germanium suggest that while the tetramer, hexamer, and heptamers of both Si and Ge are closed-shell species with "band gaps" of 1–1.5 eV, the Ge_{10} species, surprisingly and unlike the Si_{10} species, exhibits no significant HOMO–LUMO gap.[111] Bare compound clusters with $4n$ valence electrons have also been observed in the spectra of group 13/group 15 mixtures. Duncan and co-workers have carried out experiments on the In_xSb_y and In_xBi_y intermetallic clusters.[96] The In_2Sb_2, In_3Sb_3, and In_4Sb_5 species appear at moderate intensity in the spectra of In_xBi_y. We thus predict these to be oblate trigonal bipyramid (five-atom species); oblate pentagonal bipyramid, capped octahedron, or tricapped tetrahedron (seven atoms); and possibly capped dodecahedron (nine atoms). The most prominent feature in these spectra, is however, the In_3Sb_3 species, which is isoelectronic with the particularly stable Si_6 and Ge_6 clusters as well as Ga_3As_3 clusters observed by Smalley and co-workers.[112] Thus the bicapped tetrahedron or oblate octahedron are likely structures for these systems. At higher nuclearities, the In_5Sb_5 cluster is particularly prominent, which is isoelectronic with the Si_{10} and Ge_{10} clusters.

Although the structures of these $4n$-electron species cannot be confidently assigned, at present, uniquely, PSEPT does greatly limit the choices available to the systems under study, and the analogies among the several spectra studied—of single elements and compound systems—support the expectation that qualitative models such as the PSEPT will be able to provide reliable models of the electronic structure of these systems.

An interesting question for the compound clusters is the site preferences of the different atom types. Schild and co-workers[93] made some tentative assignements for the Pb_xSb_y clusters on the basis of atomic valences, but the influence of electronegativity and resonance integral changes remains to be investigated.

Clusters with More Than 4n + 2 Electrons

Ligated clusters with $5n$ valence electrons, such as $(CH)_n$, often form three-connected clusters. The clusters of group 15 elements are obvious candidates for such structures. It is well-known that the 20-electron species As_4,[113] Sb_4,[114,115] and Bi_4,[116,117] are present in the vapor above the solids, and these are obvious candidates for tetrahedral structures. P_4 is, of course, tetrahedral, Clusters of neutral and ionic group 15 elements have been reported recently.[118,119] The following geometries are predicted for the neutral higher group 15 clusters: M_6, trigonal prism; M_8, cube or cuneane; M_{10}, pentagonal prism; M_{12}, truncated tetrahedron; M_{20}, dodecahedron.

The cations of odd-nuclearity group 15 cluster are also able to adope electron-correct structures related to polyhedra. M_5^+ will have seven electron pairs and so, as Geusic et al. have suggested,[118] should be a *nido*-octahedron, while M_7^+ will adopt an arachno structure based on the tricapped trigonal prism. Geusic et al. also suggest[118] that M_6 will adopt an *arachno*-dodecahedron, but the trigonal prism is, in this case, perhaps more likely.

The tendency to form clusters increases down the group; cluster beam experiments on Sb (although not Bi) show that only clusters of nuclearity $4n$ are formed in condensation of the vapor in a noble gas, confirming the particular stability of the tetrahedral cluster,[118,119] while calculations show that the energy difference between P_4 and cubic P_8 is very small,[120] and so it is unclear whether any chemically bound clusters of phosphorus of nuclearity higher than four will form.

Clusters with $6n$ valence electrons generally form rings, and their bonding can be interpreted by using localized bond models. Sulfur provides an extensive series of clusters of this type.[89]

B. PSEPT Applied to Gas-Phase Transition-Metal Clusters

PSEPT was developed to account for the observed structures of condensed-phase, ligated clusters. Transition-metal clusters of this type are predominantly closed-shell, diamagnetic species, the narrow "band" of d orbitals being entirely filled. Bare transition-metal clusters are generally open-shell species, with a partially filled d-"band".[121] The accurate theoretical description of even the smallest of these clusters has been a great challenge for theory, with the subtle interplay of Coulombic repulsions and exchange forces making the electronic structure often finely balanced between different alternatives.[122] The role of electron-counting rules and the possibility of structural generalizations in such situations have not yet been explored.

One area where PSEPT does have an important role to play, however, is in the study of gas-phase *ligated* transition-metal clusters. In some recent very elegant molecular beam experiments Fayet, McGlinchey, and Wöste have mass-selected individual Ni_n (n = 1–20) cluster ions and studied their reactions with carbon monoxide.[123] A range of cluster ions was formed with varying numbers of carbonyl ligands and the following primary reactions were identified;

$$Ni_n^+ + kCO \rightarrow Ni_n(CO)_k^+$$

$$Ni_n^+ + lCO \rightarrow Ni_nC(CO)_l^+$$

$$Ni_n^+ + mCO \rightarrow Ni_{n-1}(CO)_m^+$$

The limiting number of carbonyls for each of these reactions as a function of the number of metal atoms is summarized in Table 7. These have been recently reinterpreted by using the principles of the PSEPT approach.[124]

It is apparent from Table 8 that $Ni_6(CO)_{13}$ and $Ni_7(CO)_{15}$ both have ($14n$ + 2) cluster valence electrons,

TABLE 7. Limiting Stoichiometries of Clusters Formed between Nickel Cluster Cations and Carbon Monoxide

limiting stoichiometry	no. of valence electrons	predicted structure
$Ni_4(CO)_{10}$	60 (15n)	tetrahedron
$Ni_5(CO)_{12}$	74 (14n + 4)	square pyramid
$Ni_6(CO)_{13}$	86 (14n + 2)	octahedron
$Ni_7(CO)_{15}$	100 (14n + 2)	pentagonal bipyramid
$Ni_8(CO)_{18}$	112 (14n)	capped pentagonal bipyramid
$Ni_9(CO)_{17}$	124 (14n - 2)	bicapped pentagonal bipyramid
$Ni_{10}(CO)_{18}$	136 (14n - 4)	tricapped pentagonal bipyramid
$Ni_{11}(CO)_{19}$	148 (14n - 6)	tetracapped pentagonal bipyramid
$Ni_{12}(CO)_{20}$	160 (14n - 8)	pentacapped pentagonal bipyramid
$Ni_{13}(CO)_{20}$	170 (14(n - 1) + 2)	centered icosahedron

TABLE 8. Limiting Stoichiometries of Clusters Formed in the Fragmentation Process $Ni_n^+ + mCO \rightarrow Ni_{n-1}(CO)_m^+$

limiting stoichiometry	no of valence electrons	predicted structure
$Ni_5(CO)_{11}$	72 (14n + 2)	trigonal bipyramid
$Ni_6(CO)_{14}$	88 (14n + 4)	nido pentagonal bipyramid
$Ni_7(CO)_{17}$	104 (14n + 6)	arachno tricapped trigonal prism
$Ni_8(CO)_{18}$	116 (14n + 4)	capped "
$Ni_9(CO)_{19}$	128 (14n + 2)	bicapped "
$Ni_{10}(CO)_{20}$	140 (14n)	tricapped "
$Ni_{11}(CO)_{21}$	152 (14n - 2)	tetracapped "
$Ni_{12}(CO)_{22}$	164 (14n - 4)	pentacapped "

as appropriate for closo structures (see above)[123] but that the subsequent clusters, with eight to twelve metal atoms, deviate from the closed-shell requirements for deltahedral clusters. The successive increments of twelve in the total number of valence electrons for these clsuters suggest that the capping principle (see above) may be appropriate[124] and that five caps are being added to the parent structure. Since the parent structure has a cluster valence electron count consistent with a pentagonal bipyramid with fivefold symmetry, this pattern suggest the growth pattern illustrated on the right-hand side of Figure 21. The pentacapped pentagonal bipyramid in Figure 21 is geometrically ideally set up to form an icosahedron with an interstitial nickel atom by the addition of one more nickel atom. According to PSEPT this centered geometry should be associated with a total of 170 valence electrons, i.e., 14 × 12 + 2. As noted above, interstitial atoms do not add to the valence electron count of these clusters. The limiting molecular species observed by Fayet and coworkers, $Ni_{13}(CO)_{20}$, has just this electron count.[123]

Such a growth sequence, based on fivefold symmetry, has previously been proposed on the basis of calculations for inert gas and metal atom clusters.[125,126]

Further support for this proposal comes from an examination of the growth sequence in the fragmentation reaction

$$Ni_n^+ + mCO \rightarrow Ni_{n-1}(CO)_m^+$$

The limiting stoichiometries of the ions observed in this process are summarized in Table 8.[123] The $Ni_6(CO)_{14}$ species has an electron count consistent with a nido structure, (14n + 4), and could most readily be accounted for in terms of a pentagonal pyramid derived from the pentagonal bipyramid by the loss of an apical atom (see Figure 22). The next member of the series, $Ni_7(CO)_{17}$, has an electron count consistent with an arachno structure and a geometry based on a tricapped trigonal prism with two adjacent vertices missing. This structure, which is illustrated in Figure 22, could also

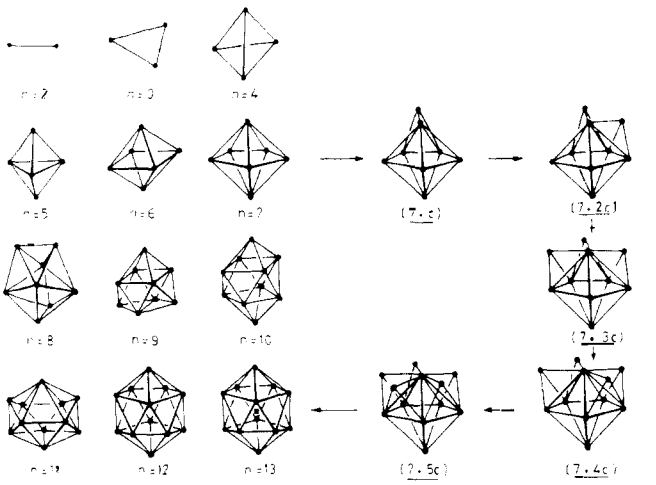

Figure 21. Capping sequence from the pentagonal bipyramid to the centered icosahedron suggested for nickel carbonyl clusters.

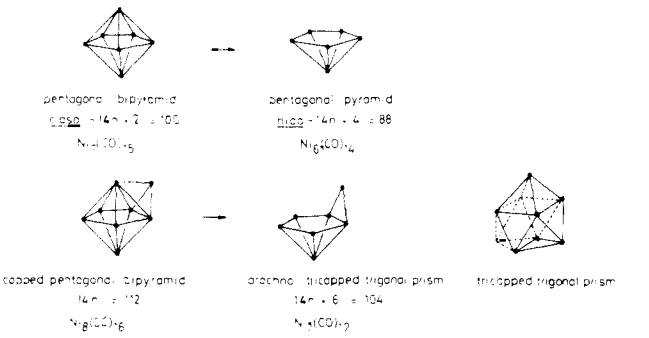

Figure 22. Proposed growth sequence for products of the fragmentation reaction of nickel clusters with CO, based on the removal of a highly connected nickel vertex from a capped structure.

be generated from a capped pentagonal bipyramid by the loss of the highest connected apical vertex, i.e., the same vertex as that lost for the pentagonal bipyramid above. Interestingly, the next five members of the series given in Table 8 have limiting electron counts that represent an increment of twelve valence electrons for each metal atom. This, of course, again suggests a series of capped molecules based on the *arachno*-$Ni_7(CO)_{17}$ structure illustrated in Figure 22.[124] These could all be derived from the capped structures illustrated in Figure 22 by the removal of a highly connected nickel vertex. The important fact is that the fragmentation pattern reinforces the growth sequence based on a pentagonal bipyramid, as described above.

In summary, PSEPT provides a consistent and unified account of the clusters observed in the molecular beam experiments when a high concentration of CO is present, although it can say little concerning the structures of clusters with few CO's.

V. Dependence of Cluster Formation on Period

We have so far generally emphasized the similarities among elements of a given group, but as the discussion of group 14 elements showed, cluster formation is also dependent on period. In particular, the chemistry of the second-row elements is, as is well-known, distinctly different from that of the heavier elements in their group.

One of the main differences observed is the preference of second-row elements, as compared to the heavier

elements in their group, to form multiple bonds. Restated, this means that second-row elements are more reluctant to adopt high coordination structures. This difference is obvious in the elements themselves. Nitrogen and oxygen form dimers, while phosphorus forms a tetrahedral P_4 unit that obeys electron-counting rules and sulfur forms eight-membered rings.[89] The thermodynamically most stable form of carbon at room temperature and below is graphite (three-coordinate) while silicon forms a diamond-like lattice. This tendency to form high coordination number species continues down the group, with lead, for instance, probably adopting a close-packed structure.

The reasons for this fundamental difference among group members is still debated; a recent article by Kutzelnigg[120] proposes that the crucial difference is that the s and p orbitals of all but second-row elements occupy significantly different regions of space (the p orbitals being more diffuse than the s orbitals) so that, despite the smaller s–p *energy* separation of the heavier elements, they are less able to hybridize.

Whatever the reason, the observation suggests that the electron-counting rules for main-group clusters will not generally apply to second-row elements, and such is indeed the case. For nitrogen and oxygen, of course, as well as the halogens, no chemically bound clusters form. For carbon, clusters have been observed over a large size range: it is known that at lower nuclearities (values of n up to at least 20) carbon forms chains and rings, no three-dimensional structures being observed. At higher nuclearities, three-dimensional structures do form, with the remarkably stable C_{60}[127] being a large, probably regular soccer ball shaped, polyhedron composed of hexagonal and pentagonal faces. The bonding in this cluster, as well as in the lower homologues, can be explained in terms of classical σ and π bonding, just as in most organic molecules.

The bonding in bare gas-phase boron clusters has been little investigated. There have been very few theoretical investigations on these species, so that no structures are currently known beyond a nuclearity of six, and even for the small clusters the structures are uncertain.[128] Only a few experimental studies of these species have been carried out to date.[128,129] It is currently unclear whether electron-counting rules have much to tell us about these $3n$ valence electron species, although preliminary extended-Hückel MO investigations suggest that closed-shell boron clusters with $n >$ 5 may adopt three-connected structures.[130] Hanley and Anderson[128] suggest that B_5^+ adopts a trigonal-bipyramidal structure.

VI. Conclusions

This review has shown how simple methods of electronic structure enable us to make predictions concerning the structures and stabilities of gas-phase clusters. The spherical jellium model and its extensions enable the prediction of many alkali-metal cluster shapes, and the analogous LCAO model of a single-shell spherical system enables us to extend these ideas to isolobal systems such as gold phosphine clusters.

Main-group clusters, both ligated and bare, exhibit more complicated stability patterns than the alkali metals. The possible structures of these clusters, for all but bare clusters of second-row elements, are severely limited by the requirements of polyhedral skeletal electron pair theory. The tensor surface harmonic theory provides the suitable zero-order spherical model that dictates the underlying electronic structures of the clusters.

There is currently little information concerning the behavior of ligated transition-metal clusters in the gas phase, but the interpretation of the nickel carbonyl clusters generated by Fayet and co-workers provides grounds for considerably optimism that here, too, the simple requirements of electron counting can guide us in our search for an understanding and prediction of the structures of these species.

Acknowledgments. We thank the SERC and the Chinese government for grants in support of this research.

References

(1) Ceriottio, A.; Demartin, F.; Longoni, G.; Manassero, M.; Marchionne, M.; Piva, G.; Sansoni, M. *Angew. Chem., Int. Ed. Engl.* **1985**, *24*, 696.
(2) Several journals have devoted issues to the subject. For example: *Chem. Rev.* **1986**, *86*, no. 3; *Surf. Sci.* **1985**, *156*, parts 1 and 2; *Ber. Bunsenges. Phys. Chem.* **1984**, *88*, 187; *Z. Phys. D* **1986**, *3*, parts 2 and 3.
(3) Herrmann, A.; Schumacher, E.; Wöste, L. *J. Chem. Phys.* **1978**, *68*, 2327.
(4) Foster, P. J.; Leckenby, R. E.; Robbins, E. J. *J. Phys. B* **1969**, *2*, 478.
(5) Echt, O.; Sattler, K.; Recknagel, E. *Phys. Rev. Lett.* **1981**, *47*, 1121.
(6) See: Kappes, M. M.; Leutwyler, S. In *Atomic and Molecular Beam Methods*; Scoles, G., Ed.; Oxford University Press: Oxford, 1987; Vol. 1.
(7) Morse, M. D.; Smalley, R. E. *Ber. Bunsenges. Phys. Chem.* **1984**, *88*, 228.
(8) Bondybey, V. E. *Science* **1985**, *227*, 125.
(9) Dietz, T. G.; Duncan, M. A.; Powers, D. E.; Smalley, R. E. *J. Chem. Phys.* **1981**, *74*, 6511. Bondybey, V. E.; English, J. H. *J. Chem. Phys.* **1981**, *74*, 6978.
(10) Sattler, K.; Mühlbach, J.; Recknagel, E. *Phys. Rev. Lett.* **1980**, *45*, 821.
(11) Powers, D. E.; Hansen, S. G.; Geusic, M. E.; Puin, A. C.; Hopkins, J. B.; Dietz, T. G.; Duncan, M. A.; Langridge-Smith, P. R. R.; Smalley, R. E. *J. Phys. Chem.* **1982**, *86*, 2556. Hopkins, J. B.; Morse, M. D.; Smalley, R. E. *J. Phys. Chem.* **1983**, *78*, 1627.
(12) For a review, see: Kappes, M. M. *Chem. Rev.* **1988**, *88*, 369.
(13) Knight, W. D.; Clemenger, K.; de Heer, W. A.; Saunders, W.; Chou, M. Y.; Cohen, M. L. *Phys. Rev. Lett.* **1984**, *52*, 2141.
(14) Whetten, R. L.; Cox, D. M.; Kaldor, A. *Surf. Sci.* **1985**, *156*, 8.
(15) Saito, Y.; Watanabe, M.; Hariwara, T.; Nishigaki, S.; Noda, T. *Jpn. J. Appl. Phys.* **1988**, *27*, 424.
(16) Knight, W. D.; Clemenger, K.; de Heer, W. A.; Saunders, W. *Solid State Commun.* **1985**, *53*, 445.
(17) Kappes, M. M.; Schür, M.; Radi, P.; Schumacher, E. *J. Chem. Phys.* **1986**, *84*, 1863.
(18) Kappes, M. M.; Schür, M.; Radi, P.; Schumacher, E. *Chem. Phys. Lett.* **1985**, *119*, 11.
(19) Kappes, M. M.; Schür, M.; Schumacher, E. *J. Phys. Chem.* **1987**, *91*, 658.
(20) Bhaskar, N. D.; Freuholz, R. P.; Klimcak, C. M.; Cook, R. A., to be published.
(21) Wang, Y.; George, T. F.; Lindsay, D. M.; Beri, A. C. *J. Chem. Phys.* **1987**, *86*, 3493.
(22) Lindsay, D. M.; Wang, Y.; George, T. F. *J. Chem. Phys.* **1987**, *86*, 3500.
(23) Lindsay, D. M.; Chu, L.; Wang, Y.; George, T. F. *J. Chem. Phys.* **1987**, *87*, 1685.
(24) For example: Hoare, M. R. *Adv. Chem. Phys.* **1979**, *40*, 49.
(25) Koutecky, J.; Fantucci, P. *Chem. Rev.* **1986**, *86*, 539–587. Pacchioni, G.; Koutecky, J. *Ber. Bunsenges. Phys. Chem.* **1984**, *88*, 242. Fantucci, P.; Koutecky, J.; Pacchioni, G. *J. Chem. Phys.* **1984**, *80*, 325–328.
(26) Martins, J. L.; Buttet, J.; Car, R. *Phys. Rev. B* **1985**, *31*, 1804.
(27) Fantucci, P.; Koutecky, K. In *Elemental and Molecular Clusters*; Benedek, G., Martin, T. P., Pacchioni, G., Eds.; Springer-Verlag: Berlin, 1988.
(28) Woods, R. D.; Saxon, D. S. *Phys. Rev.* **1954**, *95*, 577.
(29) Cohen, M. L.; Chou, M. Y.; Knight, W. D.; de Heer, W. A. *J. Phys. Chem.* **1987**, *91*, 3141.

(30) Saito, Y.; Minami, K.; Ishida, T.; Noda, T. *Z. Phys. D.* **1989**, *11*, 87.
(31) Katakuse, I.; Ichihara, T.; Fujita, Y.; Matsui, T.; Sakurai, T.; Matsuda, H. *Int. J. Mass Spectrom. Ion Processes* **1985**, *67*, 229.
(32) Katakuse, I.; Ichihara, T.; Fujita, Y.; Matsui, T.; Sakurai, T.; Matsuda, H. *Int. J. Mass Spectrom. Ion Processes* **1986**, *69*, 109.
(33) Knight, W. D.; de Heer, W. A.; Saunders, W. A.; Clemenger, K.; Chou, M. Y.; Cohen, M. L. *Chem. Phys. Lett.* **1987**, *134*, 1.
(34) Zhang, S. B.; Cohen, M. L.; Chou, M. Y. *Phys. Rev. B* **1987**, *36*, 3455.
(35) Ekardt, W. *Phys. Rev. Lett.* **1984**, *52*, 1925.
(36) Ekardt, W. *Phys. Rev. B* **1984**, *29*, 1558.
(37) Baladron, C.; Alonso, J. *Physica B* **1988**, *154*, 73.
(38) Clemenger, K. *Phys. Rev. B* **1985**, *32*, 1359.
(39) Upton, T. H. *Phys. Rev. Lett.* **1986**, *56*, 2168.
(40) Upton, T. H. *J. Chem. Phys.* **1987**, *86*, 7054.
(41) Lin Zhenyang; Slee, T.; Mingos, D. M. P. *Chem. Phys.*, submitted for publication.
(42) Griffith, J. S. *Theory of Transition Metal Ions*; Cambridge University Press: Cambridge, 1961.
(43) Silver, B. L. *Irreducible Tensor Methods*; Academic Press: New York, 1976.
(44) Hutchings, M. T. *Solid State Phys.* **1964**, *16*, 227.
(45) Wales, D. J.; Mingos, D. M. P. *Inorg. Chem.* **1989**, *28*, 2748.
(46) Stone, A. J. *Mol. Phys.* **1980**, *41*, 1339.
(47) Stone, A. J. *Inorg. Chem.* **1981**, *20*, 563.
(48) Stone, A. J. *Polhedron* **1984**, *3*, 1299.
(49) Longuet-Higgins, H. C. *Q. Rev. Chem. Soc.* **1957**, *11*, 121.
(50) Hoffman, D. K.; Reudenberg, K.; Verkade, G. G. *Struct. Bonding* **1977**, *33*, 57.
(51) Hoffmann, R.; Lipscomb, W. N. *J. Chem. Phys.* **1962**, *36*, 2179. Hoffmann, R.; Lipscomb, W. N. *J. Chem. Phys.* **1962**, *36*, 3489. Hoffmann, R.; Lipscomb, W. N. *J. Chem. Phys.* **1962**, *36*, 2872.
(52) Mingos, D. M. P.; Lin Zhenyang *Chem. Phys.* **1989**, *137*, 15.
(53) LaiHing, K.; Cheng, P. Y.; Duncan, M. A. *Z. Phys. D*, in press.
(54) Ashcroft, N. W.; Mermin, N. D. *Solid State Physics*; Holt-Saunders: Philadelphia, 1976; Chapter 10.
(55) Hall, K. P.; Mingos, D. M. P. *Prog. Inorg. Chem.* **1984**, *32*, 237.
(56) Mingos, D. M. P. *Polyhedron* **1984**, *3*, 1289.
(57) Mingos, D. M. P. *J. Chem. Soc., Dalton Trans.* **1976**, *1163*.
(58) Hall, K. P.; Briant, C. E.; Mingos, D. M. P. *J. Organomet. Chem.* **1983**, *254*, C18.
(59) van der Velden, J. W. A.; Beurskens, P. T.; Bour, J. J.; Bosman, W. P.; Noordik, J. H.; Kolenbrander, M.; Buskes, J. A. K. M. *Inorg. Chem.* **1984**, *23*, 146.
(60) Hall, K. P.; Gilmour, D. I.; Mingos, D. M. P. *J. Organomet. Chem.* **1984**, *268*, 275.
(61) Briant, C. E.; Theobald, B. R. C.; White, J. W.; Bell, L. K.; Mingos, D. M. P. *J. Chem. Soc., Chem. Commun.* **1981**, 201.
(62) van der Velden, J. W. A.; Bour, J. J.; Steggerda, J. J.; Beurskens, P. T.; Roseboom, M.; Noordik, J. H. *Inorg. Chem.* **1982**, *21*, 4321.
(63) Elian, M.; Hoffmann, R. *Inorg. Chem.* **1975**, *14*, 1058–1076.
(64) Elian, M.; Chen, M. M. L.; Mingos, D. M. P.; Hoffmann, R. *Inorg. Chem.* **1976**, *15*, 1148–1155.
(65) Hoffmann, R. *Angew. Chem., Int. Ed. Engl.* **1982**, *21*, 711–722.
(66) Bergmann, T.; Limberger, H.; Martin, T. P. *Phys. Rev. Lett.* **1988**, *60*, 1767.
(67) Scherbaum, F.; Grohmann, A.; Huber, B.; Krüger, C.; Schmidbaur, H. *Angew. Chem., Int. Ed. Engl.* **1988**, *27*, 1544.
(68) Williams, R. E. *Inorg. Chem.* **1971**, *10*, 210.
(69) Williams, R. E. *Adv. Inorg. Radiochem.* **1976**, *18*, 67.
(70) Wade, K. *J. Chem. Soc., Chem. Commun.* **1971**, 792.
(71) Wade, K. *Adv. Inorg. Radiochem.* **1976**, *18*, 1.
(72) Rudolph, R. W. *Acc. Chem. Res.* **1976**, *9*, 446.
(73) Corbett, J. D. *Chem. Rev.* **1985**, *85*, 383.
(74) Corbett, J. D. *Prog. Inorg. Chem.* **1976**, *21*, 129.
(75) Mingos, D. M. P. *Nature, Phys. Sci.* **1972**, *236*, 99.
(76) Mingos, D. M. P. *Chem. Soc. Rev.* **1986**, *15*, 31.
(77) Mingos, D. M. P.; Johnston, R. L. *Struct. Bonding* **1987**, *68*, 29.
(78) King, R. B. In *Chemical Applications of Topological and Graph Theory*; King, R. B., Ed.; Elsevier: Amsterdam, 1983; pp 99–123.
(79) Teo, B. K. *Inorg. Chem.* **1984**, *23*, 1251.
(80) Teo, B. K.; Longoni, G.; Chung, F. R. K. *Inorg. Chem.* **1984**, *23*, 1257.
(81) von Schnering, H. G. *Angew. Chem., Int. Ed. Engl.* **1981**, *20*, 33.
(82) Martin, T. P. *Angew. Chem., Int. Ed. Engl.* **1986**, *25*, 197.
(83) Herrmann, W. H. *Agnew. Chem., Int. Ed. Engl.* **1986**, *25*, 56.
(84) McPartlin, M. *Polyhedron* **1984**, *3*, 1279.
(85) Mingos, D. M. P. *J. Chem. Soc., Chem. Commun.* **1983**, 706.
(86) Mingos, D. M. P.; Evans, D. G. *J. Organomet. Chem.* **1983**, *251*, C13.
(87) Hopkins, J. B.; Langridge-Smith, P.; Morse, M. D.; Smalley, R. E. *J. Chem. Phys.* **1983**, *78*, 1627.
(88) For a review, see: Bloomfield, L. A. In *Physics and Chemistry of Small Clusters*; Jena, P., Rao, B. K., Khanna, S. N., Eds.; NATO ASI Series B; Plenum Press: New York, 1987; Vol. 158, p 219.
(89) Martin, T. P. *J. Chem. Phys.* **1984**, *81*, 4426.
(90) Martin, T. P. *Z. Phys. D* **1986**, *3*, 211.
(91) Wheeler, R. G.; LaiHing, K.; Wilson, W. L.; Allen, J. D.; King, R. B.; Duncan, M. A. *J. Am. Chem. Soc.* **1986**, *108*, 8101.
(92) Wheeler, R. G.; LaiHing, K.; Wilson, W. L.; Duncan, M. A. *J. Chem. Phys.* **1988**, *88*, 2831.
(93) Schild, D.; Pflaum, R.; Sattler, K.; Recknagel, E. *J. Phys. Chem.* **1987**, *91*, 2648.
(94) Lohr, L. *Inorg. Chem.* **1981**, *20*, 4229–4235.
(95) Guggenberger, L. J. *Inorg. Chem.* **1968**, *7*, 198.
(96) Bishop, M. B.; LaiHing, K.; Cheng, P. Y.; Peschke, M.; Duncan, M. A. *J. Phys. Chem.* **1989**, *93*, 1566–1569.
(97) Mingos, D. M. P.; Johnston, R. L. *Struct. Bonding* **1986**, *68*, 29.
(98) Slee, T.; Lin Zhenyang; Mingos, D. M. P. *Inorg. Chem.* **1989**, *28*, 2256.
(99) Raghavachari, K. *J. Chem. Phys.* **1985**, *83*, 3520.
(100) Raghavachari, K. *J. Chem. Phys.* **1987**, *84*, 5672.
(101) Raghavachari, K.; McMichael-Rohlfing, C. *J. Chem. Phys.* **1989**, *89*, 2219.
(102) Bloomfield, L. A.; Freeman, R. R.; Brown, W. L. *Phys. Rev. Lett.* **1985**, *54*, 2246.
(103) Heath, J. R.; Liu, Y.; O'Brien, S. C.; Zhang, Q.-L.; Curl, R. F.; Tittel, F. K.; Smalley, R. E. *J. Chem. Phys.* **1985**, *83*, 5520–5526.
(104) Trevor, D. J.; Cox, D. M.; Reichmann, K. C.; Brickman, R. O.; Kaldor, A. *J. Phys. Chem.* **1987**, *91*, 2598–2601.
(105) Phillips, J. C. *J. Chem. Phys.* **1985**, *83*, 3330.
(106) Phillips, J. C. *Chem. Rev.* **1986**, *86*, 619.
(107) Feuston, B. P.; Kalia, R. K.; Vashishta, P. In *Physics and Chemistry of Small Clusters*; Jena, P., Rao, B. K.; Khanna, S. N., Eds.; NATO ASI Series B; Plenum Press: New York, 1987; Vol. 158, p 283.
(108) Ohnishi, S.; Saito, S.; Satoko, C.; Sugano, S. In *Physics and Chemistry of Small Clusters*; Jena, P., Rao, B. K.; Khanna, S. N., Eds.; NATO ASI Series B; Plenum Press: New York, 1987; Vol. 158, p 235.
(109) LaiHing, K.; Wheeler, R. G.; Wilson, W. L.; Duncan, M. A. *J. Chem. Phys.* **1987**, *87*, 3401–3409.
(110) (a) Ding, A.; Hesslich, J. *Chem. Phys. Lett.* **1983**, *94*, 54. (b) Mackay, A. L. *Acta Crystallogr.* **1962**, *15*, 916.
(111) Cheshnovsky, O.; Yang, S. H.; Pettiette, C. L.; Craycraft, M. J.; Liu, Y.; Smalley, R. E. *Chem. Phys. Lett.* **1987**, *138*, 119.
(112) O'Brien, S. C.; Liu, Y.; Zhang, Q.; Heath, J. R.; Tittel, F. K.; Curl, R. F.; Smalley, R. E. *J. Chem. Phys.* **1986**, *84*, 4074.
(113) McGonigal, P. J.; Grosse, A. V. *J. Phys. Chem.* **1963**, *67*, 924.
(114) Illarinan, V. V.; Charepanova, A. S. *Dokl. Akad. Nauk SSSR* **1960**, *133*, 1086.
(115) Rosenblatt, G. M.; Birchenallis, C. E. *J. Chem. Phys.* **1961**, *35*, 788.
(116) Rovner, L.; Drowart, A.; Drowart, J. *Trans. Faraday Soc.* **1967**, *63*, 2906.
(117) Kohl, J. F.; Uy, O. M.; Carlson, K. D. *Chem. Phys.* **1967**, *47*, 2667.
(118) Geusic, M. E.; Freeman, R. R.; Duncan, M. A. *J. Chem. Phys.* **1988**, *89*, 223.
(119) Ross, M. M.; McElvany, S. W. *J. Chem. Phys.* **1988**, *89*, 4821.
(120) Kutzelnigg, W. *Angew. Chem., Int. Ed. Engl.* **1984**, *23*, 272.
(121) Morse, M. D. *Chem. Rev.* **1986**, *86*, 1049.
(122) Salahub, D. R. *Adv. Chem. Phys.* **1987**, *69*, 447.
(123) Fayet, M.; McGlinchey, M. J.; Wöste, L. H. *J. Am. Chem. Soc.* **1987**, *109*, 5305.
(124) Mingos, D. M. P.; Wales, D. J. *J. Am. Chem. Soc.*, in press.
(125) Burton, J. J. *Catal. Rev.* **1977**, *9*, 209.
(126) Hoare, M. R.; Pal, P. *Nature, Phys. Sci.* **1972**, *236*, 35.
(127) Kroto, H. W.; Heath, J. R.; O'Brien, S. C.; Curl, R. F.; Smalley, R. E. *Nature* **1985**, *318*, 162.
(128) Hanley, L.; Anderson, S. L. *J. Phys. Chem.* **1987**, *91*, 5161–5163.
(129) Hanley, L.; Anderson, S. L. *J. Chem. Phys.* **1988**, *89*, 2848. Hanley, L.; Whitten, J. L.; Anderson, S. L. *J. Phys. Chem.* **1988**, *92*, 5803–5812.
(130) Slee, T., unpublished work.